2023

STUDY OF DROPLETS INTERACTIONS ON SOLID SURFACE FOR MANUFACTURING APPLICATIONS

Menghan Zhao
Michigan Technological University, zmenghan@mtu.edu

STUDY OF DROPLETS INTERACTIONS ON SOLID SURFACE FOR MANUFACTURING APPLICATIONS

By

Menghan Zhao

A DISSERTATION

Submitted in partial fulfillment of the requirements for the degree of

DOCTOR OF PHILOSOPHY

In Mechanical Engineering-Engineering Mechanics

MICHIGAN TECHNOLOGICAL UNIVERSITY

2023

This dissertation has been approved in partial fulfillment of the requirements for the Degree of DOCTOR OF PHILOSOPHY in Mechanical Engineering-Engineering Mechanics.

Department of Mechanical Engineering-Engineering Mechanics

Dissertation Advisor:	*Dr. Kazuya Tajiri*
Committee Member:	*Dr. Song-Lin Yang*
Committee Member:	*Dr. Zhen Liu*
Committee Member:	*Dr. Jeffrey S. Allen*
Department Chair:	*Dr. Jason R. Blough*

Table of Contents

List of Figures

List of Tables

Author Contribution Statement

A peer-reviewed conference proceeding paper.

Oscillation dynamics of droplet's impact on a solid surface: frequencies, damping, and bouncing, ASFET 2022

Spreading and oscillation of single droplet impact on a solid substrate, HEFAT 2021

Acknowledgments

I want to thank my advisor, Dr. Tajiri, for guiding me and helping me since 2017. Without his guidance, encouragement, patience, and support, my research career would have irreversibly fallen into blindness and chaos, and this dissertation will never have been done.

I would also like to thank my committee members, Dr. Yang, Dr. Liu, and Dr. Allen; your patience and kindness will be appreciated in my life.

I also have a special thanks to my friends, Karrar T. Alofari, Udit Sharma, Shahab Bayani, and Kishan Bellur. Your helped solve a lot of problems in my research path.

Definitions

We	[~]	Weber number
Re	[~]	Reynolds number
σ	[mN/m]	surface tension
ρ	[kg/m3]	density
μ	[Pa*s]	dynamic viscosity
u	[m/s]	impact velocity
D	[mm]	droplet diameter
β	[~]	droplet flatness
Amp_{beta}		oscillation amplitude of flatness
ω	[1/s]	oscillation frequency

List of Abbreviations

DHO	damped harmonic oscillator
DI	deionized water
P03	deionized water mixture with 3% volume of n-propane alcohol
P05	deionized water mixture with 5% volume of n-propane alcohol
P10	deionized water mixture with 10% volume of n-propane alcohol
CA	contact angle
SFT	surface tension
STD	standard deviation

Abstract

Droplet impact behaviors on a solid substrate are a complicated process that involves multiple phenomena on a small scale within a short time. This phenomenon has wide applications in the industrial, medical, and scientific fields. Researchers select the oscillation process as the marked phase to observe and analyze the dynamical balancing between different forces and conservation of energies and compare it to the typical damped harmonic oscillator (DHO) model to examine the character of variables such as viscosity, surface tension, and wettability. The testing results lead to the creation of a precise model for post-impact dynamics, describing how the solid wettability (which is demonstrated as the contact angle) and the surface tension (which is presented as the weber number) help control the oscillation dynamics. Further studies reveal the influence of the weber number on oscillation frequencies and make a capillary pressure related assumption about satellite droplet separated from the main body. The latest study reveals the influence of viscosities on the dynamics. Researchers create the overall functions of the Weber number and Reynolds number to create a model that can represent the oscillation process under a wide range of conditions.

1 Introduction

From rainfall on the lotus's leaves to the 3D printing material deposited on the working plate, the droplet's impact behaviors are one of the most common phenomena in daily life and industrial applications. For the fuel injection of the internal combustion engine, the diesel drops attached to the chamber's wall are harmful to the engine's emissions as well as the fuel efficiency; for thermal spray technology, the drop's stability after deposition will determine the working efficiency and manufacturing speed; for spray cooling system, the size and impact velocities of water drop on the cooling surface will determine the heat exchanger efficiency.

Based on the applications of related studies, the research of this problem can be regulated by different dimensions: thermal dynamics analysis, fluid mechanical studies, chemical reactions, and surface energy issues.

In the fuel cell-related industry, especially the catalyst layers manufacturing, the inkjet printing coating is one of the most promising manufacturing strategies. The ink's deposition distance is based on the droplet's maximum or equilibrium spreading diameter. That factor is determined by multiple parameters, including the liquid's viscosity, surface tension, impact velocity, density, and size, the solid materials' wettability, roughness, and the environments such as humidity and temperature.

1.1 Applications of Droplet impact on a solid substrate

The interaction between a liquid drop and solid substrate can be concerned as a Crossfield of multi-phases, multiple physics, and multi-scale problems. Today this phenomenon is widely studied and further discussed, thanks to the thriving applications in industry, such as the icing on the wing in aircraft flight, inkjet printing, fast 3D printing, spraying coating cooling, and fuel jetting in Internal combustion engine cylinders, and turbine engine's design.

1.1.1 Spraying coating

The thermal spray is one of the most valuable applications of droplet behavior study. Metal or ceramic powders are used as material deposited on the substrate to coat the thermal barrier and resistances. Here is the manufacturing process: first, power is injected from the blower, then the powder spray will flow through a layer of high-temperature gas, which melts the powder into liquid droplets, atomize the drops and accelerate them. After that, the droplets will be deposited onto the chipboard, form the coating splat leeringly, layers after layers of splat will finally create the coating. Research[1-6] of this application shows that during the process, variables such as powders' flow velocities, mass flow rate, trajectory, and sizes are important for manufacturing quality and speed, environmental factors such as gas temperature, and the solid substrate's roughness and temperature are also critical for the coating.

1.1.2 Spraying cooling

Another application that involves the thermal process during droplet behavior is spraying cooling. By jetting low coolant such as water on a high-temperature solid substrate, this method use vaporization to improve the heat transfer. During the

process, the droplet's size is the primary factor that determines the whole efficiency. Besides liquid's heat capacity[7-11], density and impact velocity also influence the heat exchanging effectiveness. Such technology has a remarkable wide range of applications, including cooling in high-performance electronic devices, steel/metal manufacturing, hot strip mill casting, fire protection, etc. One technique challenge of this application is maintaining the heat flux uniformities[12-14]. Such requirement demands precise control of drop deposition, size, and velocities.

1.1.3 IC engine fuel spraying

One frequently studied field for a direct injection combustion engine is the fuel impingement behaviors on cylinder walls and pistons. This phenomenon can severely increase the emission and reduce the efficiency of engine[15-19]. Therefore, the studies of fuel attachment have significant importance for both economic and environmental concerns. Recent studies also focused on applications of super-hydrophobic coating in the combustion chamber, which help the enhancement of engines' performance[20-24]. So, this topic is also related to the super-hydrophobic impact behaviors studies.

1.1.4 Microfluidic

The most common application of droplet behaviors on the solid surface is the designation and optimization of microfluidic devices. This is widely used in food production, chemical industry, medicine, biological industry, environmental studies[25-27], etc. the small scales of such devices require high flow control accuracy. Thus the droplet is selected as the method of liquid transportation.

1.1.5 Inkjet printing

Inkjet printing technologies are based generation and deposition of micro-scale droplets; therefore, the development of these technologies depends on heavy studies of micro-scale droplets and their behaviors on fiber substrates. The motivation for understanding the dynamics of drop interactions of the substrate is to increase the positioning accuracy, optimize the volume of ink drop, reduce the consumption of ink, prevent the problem such as droplet rebounding, improve the printing speed as well as enhance the printing qualities such as the uniformities[28-30].

1.2 Dimensions and parameters which influence the dynamics of drop impact.

Despite the complicated impact dynamics, the whole process can be reviewed as the energy converges between surface energy (for different surfaces and materials), kinetic energy, and thermal energy. Therefore, the primary variables in the study should be the properties of liquid, especially the surface tension, as well as the surface conditions (such as wettability) of solid material. To unify the analysis, the whole process will be described by only dimensionless parameters, such as maximum spreading factors, flatness, dimensionless time, etc[31-33].

Several dimensionless parameters have been commonly used in research to examine the process of drop's impact behaviors. The forces or types of energy determine the importance of these parameters. Due to the surface tension of liquid dominating the dynamic, dimensionless parameters containing the surface tension will be selected as the pre-conditional factors. The bond number represents the gravity effect of a droplet compared to the drop's surface tension, the high bond number means the drop's shape

and static will be influenced by gravity significantly, which makes the behaviors more complicated. In dynamics, the most critical parameter for this study is the Weber number, defined as the droplet inertia ratio over the surface tension. Besides, to analyze the influence of viscosity, Reynolds number and Capillary numbers are also concerned in this study.

Table 1. Dimensionless parameters of the droplet impact study

Dimensionless parameters	Formulations	Definitions
Weber number	$We = \frac{\rho v^2 D}{\sigma}$	Kinetic over surface tension
Reynolds number	$Re = \frac{\rho v D}{\mu}$	Inertia over viscosity
Ohnesorge number	$Oh = \frac{\sqrt{We}}{Re} = \frac{\mu}{\sqrt{\sigma \rho D}}$	Viscosity to inertia and surface tension
Capillary number	$Ca = \frac{\mu V}{\sigma}$	The ratio between drag force and surface tension force
Bond number	$Bo = \frac{\rho g D^2}{\sigma}$	Weight over surface tension

Dimensionless time	$\tau = \frac{tV}{D_{drop}}$	Actual time to spreading time
Spreading ratio	$S = \frac{D_{spread}}{D_{drop}}$	Spreading diameter to drop diameter
Flatness	$\beta = \frac{H}{D_{spread}}$	Droplet height over spreading diameter

1.3 Conditions of droplet behaviors studies

1.3.1 Types of droplet impact behaviors on the solid substrate

As a compilation of complicated phenomena driven by multiple physics under various combinations of conditions, the impact behaviors have three types: Deposition, Splash, and Rebounding[31, 32, 34-38]

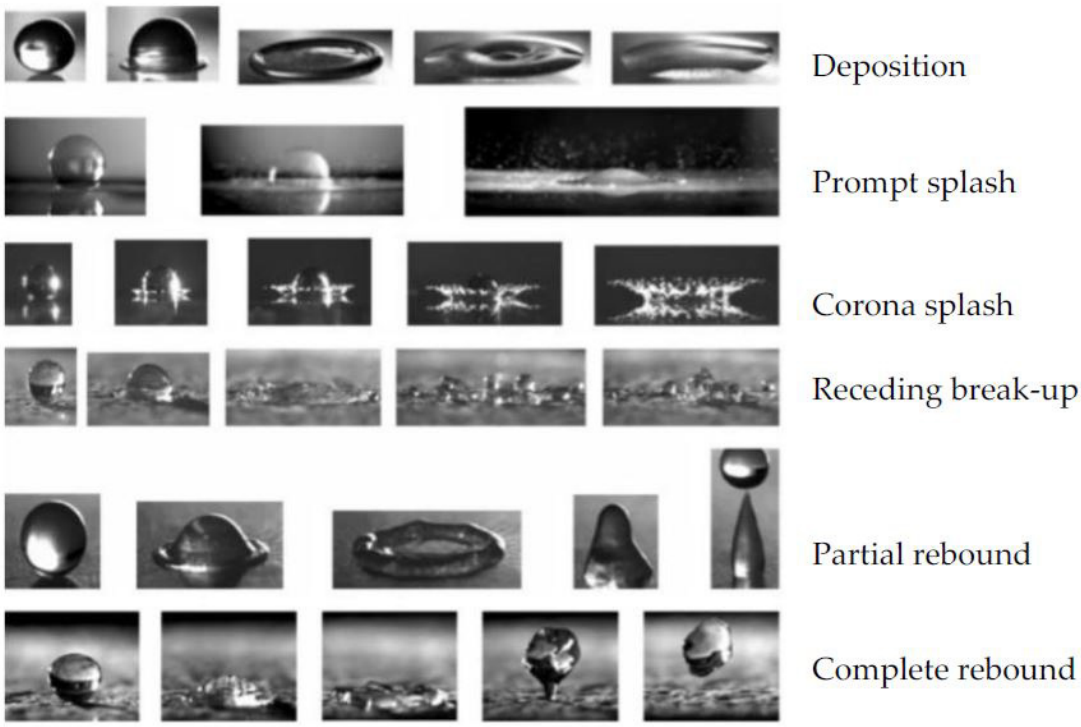

Figure 1. Droplet's impact regime on solid substrate[39]

For industrial application concerns, the expansion of the impact droplet's regime is the most cortical parameter to be observed. Yet, other parameters such as oscillation delaying time are also attractive to some researchers. The maximum spreading diameter is considered the most critical due to the potential heat transfer on the contact area and the transfer between different types. Like the dimensionless parameters above, the spread ratio represents the maximum spread[40-43].

There are multiple expressions of the maximum spreading ratio by different dimensionless parameters, shown as follow:

Asai[43]

$$S_{max} = 1 + 0.48We^{0.5} \times \exp\left[-1.48\ We^{0.22}\ Re^{-0.21}\right]$$

Chandra and Avedisian [44]

$$\frac{3We}{2Re}S_{max}^4 + (1 - cos\theta)S_{max}^2 - \left(\frac{We}{3} + 4\right) = 0$$

Jones[45]

$$S_{max} = \sqrt{\frac{4}{3}Re^{1/4}}$$

Mao et al.[46]

$$\left[\frac{1}{4}(1 - cos\theta) + 0.2\frac{We^{0.83}}{Re^{0.33}}\right]S_{max}^3 - \left(\frac{We}{12} + 1\right)S_{max} + \frac{2}{3} = 0$$

Pasandideh-Fard et al.[47]

$$S_{max} = \sqrt{\frac{We + 12}{3(1 - cos\theta_A) + 4\left(We/\sqrt{Re}\right)}}$$

Ukiwe and Kwok[48]

$$(We+12)\,S_{max} = 8 + S_{max}^{3} \times \left[3(1-cos\theta_A) + 4\frac{We}{\sqrt{Re}}\right]$$

After the maximum spreading, the droplet starts receding. The surface tension drives the droplet's receding; when the droplet impact velocity is higher than a certain threshold, the spreading ratio is beyond the surface tension's ability to maintain the droplet's shape, which leads to splash.

There are multiple types of splash: prompt splash, in which droplets disintegrate, and minor satellites as the "secondary" droplets are jetted out after the impact immediately; corona splash, in which the rim of the droplet lifts off the surface and forms a crown, and the secondary drops are separated from the crown; break-up, in which the spreading regime is the stellar shape and patterns from the sharp edge separated from the droplet and formed the secondary drops.

Besides splash, another interesting topic that has been heavily studied is rebounding. This phenomenon commonly occurs at the impact of hydrophobic or super-hydrophobic surfaces. An interesting dynamic to be explored carefully is the bounding as a function of dimensionless numbers is not monotonous; for example, fully rebounding only occurs at a "medium' velocity regime. And sessile satellite droplets only jetted out at low impact velocities regime. It is also worth to noticed that the air bubble trapped beneath the drop during the initial impact has a highly unregulated and unpredicted influence on the spreading ratio and bounding.

1.3.2 Phases of droplet deposition on the solid substrate

By analyzing the droplet's impact behaviors, the whole process can be divided into four phases: kinematic phase, spreading phase, oscillation/relaxation phase, and equilibrium phase. Those phases can be reviewed as dynamical balancing between several forces and different types of energies.

The kinematic phase is the initial contact between the liquid and solid. In the first impact phase, the mechanism is mainly driven by inertia. Surface tension, interfacial tension, and van de Waals forces play minor roles due to the limited contact surface.

After the initial contact, the droplet continues to spread on the surface. The process from initial contact to maximum spreading is the spreading phase. During this phase, the drop's oscillations show significant differences from hydrophilic to hydrophobic surfaces: for high surface energy material, such as glass or acrylic, a thin film (thickness less than 50 nm) can be formed around the drop, and it spread faster than the droplet's visible edge. As a result, these conditions' dynamic contact angle variation has been minimized. Yet, the spreading phase is far more complicated for the hydrophobic surface material, and a torus ring structure will form as the advanced dynamic contact angle is reached. The formation and regulation of torus depend on multiple factors, including impact velocities, surface wettability, viscosities, and surface tension. Substrates' roughness and stiffness also play roles in these dynamics

After the maximum spreading, the process is followed by an oscillation/relaxation phase. This phase oscillates between geometrical parameters, especially the drop's height. Theoretically, the oscillation is like the spring stiffness mode or RLC circuit:

here, the constant stiffness k, which plays as the force of resistance of shear, and determines the oscillation's frequencies, is replaced by the parameter of surface tension and interfacial tensions. The decaying ratio, which controls the duration of oscillation, is like the inner forces of liquid; such forces can consume the kinetic energy. For low bond number conditions, the impact of the drop's mass and size is relatively minor compared to the solid substrate's wettability.

1.4 Rigid solid surface

For most applications in industry, the droplet impact will be performed on relatively stable solid substrates. Thus, movements like vibrations of a solid surface are negligible, and droplets' impact velocities can be simplified as constants; studies of this type of case will mainly focus on the liquid side rather than solid properties.

1.4.1 Temperature influences the behaviors

The temperature has an influence on the dynamics from multiple aspects. The surface energy of both liquid and solid are sensitive to the temperature; further temperature change can involve liquid's phase change, including evaporation, condensing, and freezing.

For a high-temperature surface, the dynamics can be divided into different regimes: evaporation, nucleate boiling, foaming, transition, and film boiling, as the temperature increases. For nucleate boiling, when drops initially contact the high-temperature solid surface, several satellite bubbles occur at nucleated locations, then these bubbles will rise and disturb the drop's shape. As the temperature increases, the dynamics go into

the regime of foaming, in which the nucleate bubble becomes big enough to interrupt the whole droplet and make it foam. Yet, the bubbles are still separated and trapped in the drop due to the surface tension. In the transition regime, the solid surface's high temperature helps the bubbles to generate and develop very fast, and the rampaging bubbles finally have enough size to break the drop's surface. Bubbles' coalescing, drop surface's break up and satellite drops generated in the process make this regime extremely unstable. Finally, a further increase in the solid temperature will drive the phenomenon into the last regime, known as film boiling. Due to the solid substrate's extremely high temperature, vaporization occurs at the initial contact of liquid and solid and develops significantly fast. A layer of vapor is formed between the drop and solid surface, which is dynamically stable. As a result, the drop is levitated from the solid. This phenomenon is heavily studied as the Leidenfrost effect. Under this phenomenon, the vapor layer also prevents the drop from rebounding.

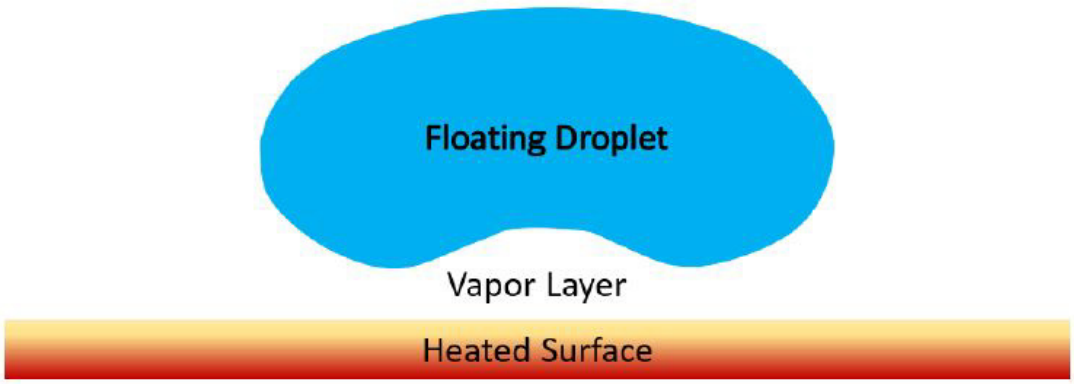

Figure 2.Leidenfrost effect on a superheated solid surface

Another temperature influence is cooling or super cooling on the solid surface. Freezing on the surface can be split into five stages: Cooling stage, where the drop

initially contacts the solid surface and starts to cool from the initial temperature to a point below the equilibrium freezing temperature. Nucleation stage, where ice crystal nucleation is formed separately. Recoalesce stage, where crystals grow rapidly from the nucleates. In the freezing stage, where the heat transfer from the solid enhances the crystal's growth, the whole drop has been frozen and solidified. Finally, in the solid cooling stage, the temperature of the solidified drop continuity decreases until it reaches the same temperature as the substrate.

1.4.2 Surface Energy/Wettability to the behaviors

Surface energy is the main factor of solid material's wettability, defined as a solid surface's ability to be wetted. Theoretically, the surface wettability is only influenced by the solid material's chemical composition and roughness. There are two states of the wet regime of drop on the solid surface. Wenzel state describes the water penetrating the micro-scale rough structures on a solid substrate and conforming to the base surface; Cassie-Baxter state shows the drop is held on the tip of roughness and maintained above the base surface[49].

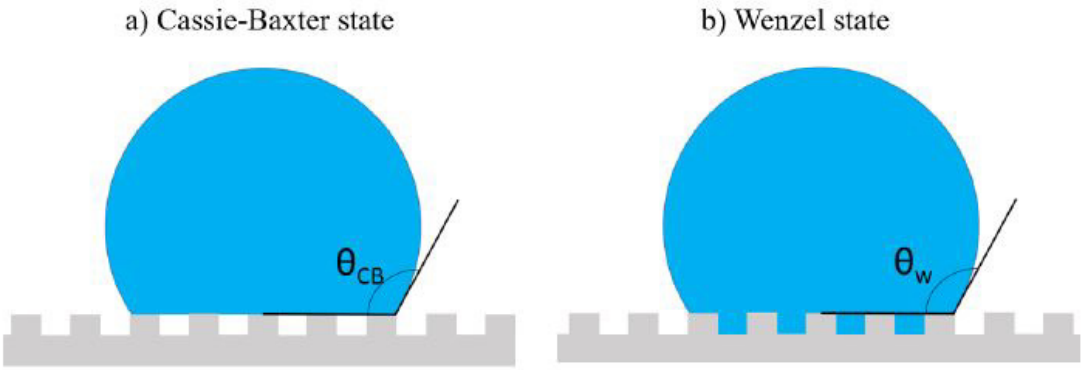

Figure 3. Wetting regimes of the droplet on a solid surface: (a) Cassie-Baxter state and (b) Wenzel state [49]

To observe and measure wettability, the most used parameter is contact angle. Static constant angle is the angle between a liquid's boundary and a wetted solid regime under a steady state. This angle can be reviewed as the result of balancing between liquid's surface tension, solid to gas/vapor interfacial tension, and solid-liquid interfacial tension. as Young's equations show:

$$\gamma_{SG} - \gamma_{SL} - \gamma_{LG} \cos\theta_C = 0$$

To formatting the solid wettability of water, the surface with a static contact angle low than 90 deg is denied as a hydrophilic surface, and a static contact angle higher than 90 deg is called a hydrophobic surface; an exceptional condition is sup-hydrophobic when the static contact angle is higher than 150 deg.

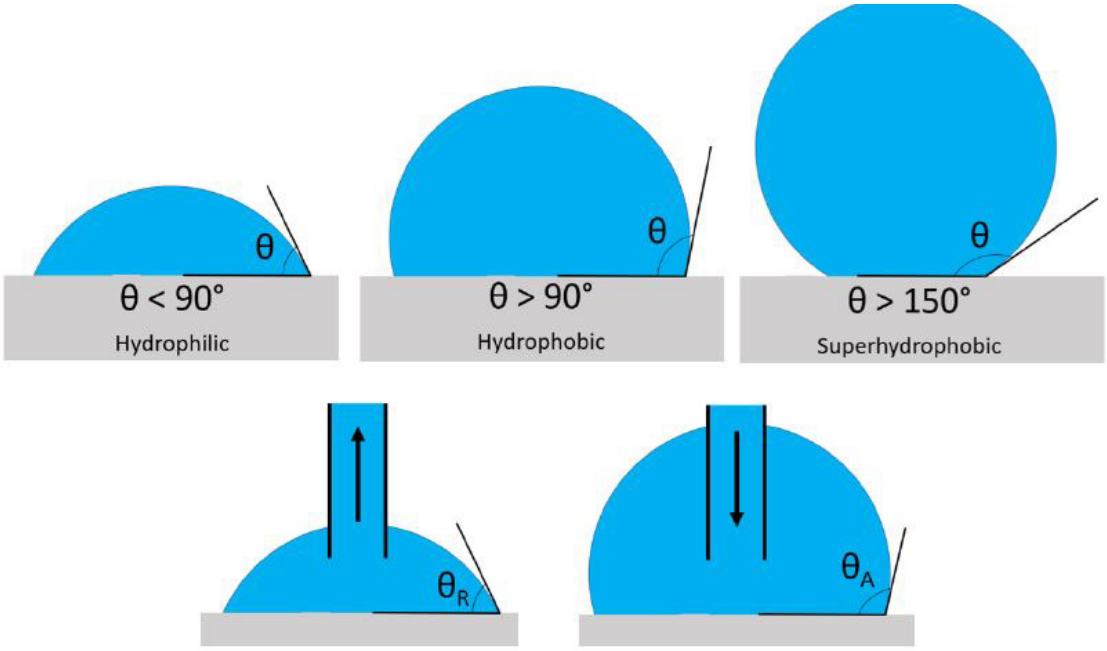

Figure 4. The contact angle of the different surfaces, advancing and receding[50]

it is necessary to notice that the contact angle is not possible to constant when the droplet is moving on a solid surface. Therefore, the dynamic contact angle is also used in such studies. The contact angle at maximum spreading speed is called the advancing contact angle, which is also the highest contact angle the drop can hold; on the other hand, the minimum contact angle when the droplet is receding from the maximum spreading is defined as the receding contact angle.

Wettability is one of the most critical parameters that influence the whole problem. Based on the previous studies, the maximum spreading diameter after a droplet's impact is determined by the solid's wettability, when a low wettability surface provides lower spreading ranges. Oscillation damping will also take a longer time to stabilize the droplet finally. This is since lower wettability provides less capacity to absorb the kinetic energy of oscillation. Since surface roughness is the main factor in determining the wettability, increasing the surface's roughness, the droplet's splash can be promoted at low Ohnesorge number conditions[51].

When considering the temperature change problems during the process, wettability significantly affects the heat transfer coefficient[41]. On the cold surface, the droplet's freezing time depends on the wettability; a low wettable surface will take longer to freeze the drop due to the lower contact area for convection. Besides, oscillation on a soft wettable surface takes a longer time to neutralize, preventing the crystal from forming within the droplet. On the other hand, the hydrophilic droplet surface has a thinner height and vast convection area, and the stability of the drop also helps the crystal form.

Similar to the freezing process, high wettability also enhances the boiling of droplets on the solid substrate. A hydrophilic surface helps smaller and faster bubble growth[52-54]. Kim's[54] work shows the wettability influence on the Leidenfrost effect. Droplets on a hydrophilic surface require lower Leidenfrost temperature because the high contact area allows the droplet to be heated faster, which makes vapor film easier to form. However, to ensure the droplet rebounding on the surface, the hydrophobic surface requires lower temperature because lower wettability requires lower extra energy to separate liquid from the solid substrate.

1.4.3 Relative humidity's influence on the behaviors

Relative humidity in specified cases has a significant influence on the solid surface's wetting, as well as the impact dynamics. For catalyst layers of fuel cells, as the relative humidity changes, the contact angle of water drop on the membrane also increases. Since wettability is one of the critical parameters of impact behaviors, it is considered that relative humidity indirectly influences the dynamics. For temperature or phase change cases, such influence is more significant. Bobinski[55]'s work reveals the experimental studies of the droplet freezing at maximum spread under high relative humidity conditions; such phenomena can be avoided by reducing the relative humidity of the environment.

Jadidi's [56]work of experimental study also helps us to understand the effect of relative humidity. When the environment temperature is close to or lower than dew temperature, relative humidity reaches the maximum, and water condensation occurs.

The droplet spreading diameter has significantly increased due to solid substrates' higher wetting conditions.

1.4.4 Impact velocities and shape

Impact velocity is one of the most important characteristics which determine the impact's type and influence the dynamics. Higher impact velocity can deliver more kinetic energy into the droplet, which enhances the spreading, and also improves the heat transfer on the surface (for the temperature changed conditions)[36, 40, 41, 57-59] When the droplet contains extra kinetic energy, the impact will shift from "moderated" deposition to "rampage" splash. It is worth mentioning that the oscillation frequencies after the impact and the receding speed after the impact also depend on the velocity. However, such functions are not always monotonous. For example, rebounding on the super-hydrophobic surface is completely at a relatively low-velocity region, yet the rebounding becomes partial at a higher impact velocity regime. Simple analyses like kinetic energy cannot explain such a phenomenon. Therefore, further studies are required to explore the details of such uncommon behaviors.

A droplet's shape is also critically important to its behaviors, yet it is also the most unpredictable factor in the dynamics. Spreading from an asymmetric droplet has a lower impact velocity threshold to splash than the round droplet[60-63]. At the rebounding regime[64], as symmetricity decreases, the droplet oscillation or rebounding height is also reduced,

1.4.5 Dimensionless parameters

Due to the importance of surface tension, this phenomenon's most critical dimensionless parameter is the Weber number. Bond number and Capillary number also play essential roles in the dynamics. By reducing the Weber number, the droplet's spreading ratio damped faster, yet the maximum spreading ratio is independent. Yet, the Bond number has almost negligible influence on the spreading ratio change. Increasing the Reynolds number, on the other hand, can promote the spreading.

1.4.6 Unstable solid surface

There are multiple methods of moving: horizontal shift, vibration, and rotation. When a solid substrate is moving, the conditions of droplet impact behaviors change due to the extra kinetic energy received from the solid. Works from Povarov's studies [65] reveal the mechanism of the air layer between liquid and solid, which is trapped by the moving of the solid surface. The droplet can lift off and rebound from the solid surface due to the air layer. As the velocities increase, the layer has a more significant effect on the drop's lift-off on solid, leading to partial rebound, fully rebound, and finally, droplet's deformation. Another study from Mundo[66]'s group shows the influence of the solid's moving speed on the threshold of a droplet's splash regime. Research from Zen[67] reveals the splash dynamics on moving surfaces. Two types of splashes: side splash and round splash, occur in different conditions. The splash threshold from round to side is determined by velocity triangles (vector of droplet's impact velocity and surface's moving velocity).

1.5 The motivation for this study

The study of droplet impact dynamics is directly based on the need for inkjet printing technologies. To manage the ink's consumption, it is necessary to examine the droplet's size, maximum spreading diameter, and duration of droplet's stability. For either the continuous or drop-on-demand method, the deposition distance between drops shall be designed based on the drop's spreading diameter, which decays after the spreading phase.

As we further studied the impact process, details of mechanisms show unpredicting roles in practice. For example, the solid substrates' wettability varies with the accumulation of drop depositions, which changes the equilibrium contact angle at the end of the impact; such mechanisms still need to be further examined; impact on the hydrophobic surface (especially the surfaces which make the equilibrium contact angles more prominent than 120 degrees) may cause drop's bouncing. However, high impact velocity doesn't; cause fully bouncing; that phenomenon only occurs in a short range of impact velocity, which is still unrevealed. Moreover, a low-velocity impact on a hydrophobic surface can cause satellite drop separation from the main drop, but such separation will not occur on higher impact velocities. These phenomena appear only by further study of the impact mechanisms.

By analyzing the drop's oscillation, stabilization, and maximum spreading diameter, the printing process of ink jet-related manufacturing or fast 3d printing technologies can be further optimized.

1.6 Structure of this document.

In this article, we will discuss the dynamics by different objectives: in chapter 2, we will briefly discuss the basic experimental setting of research, including the selection of liquid, solid material, environmental conditions, and impact controls.

In chapter 3, we will discuss the oscillation and damping factors of droplets' height and diameter at post-impact phases, significantly how the surface energies of different solid materials and the surface tension of liquids change the oscillation process. Studies will mainly focus on the influence of weber number and contact angles.

In chapter 4, Our studies will reveal the mechanism of oscillation frequencies as functions of liquid surface tension and contact angles. The oscillation frequencies change nonlinearly and non-monotonically as functions of weber number and the equilibrium contact angles; oscillation behaviors also show significant differences on hydrophobic and hydrophilic surfaces; the satellite drop's separation, and jetting will also be analyzed precisely.

In chapter 5, We will analyze the influence of viscosities on impact mechanisms. Especially the contact angle's variation and oscillation behaviors. These studies will include a broader range of impact velocities and focus on the Reynolds' number determination of the damping and oscillation frequencies. A modification of the capillary waves model will also be discussed.

Finally, in chapter 6, we will conclude all these studies above, creating universal dynamics of geometrical factors (flatness, maximum spreading factors, dynamic contact

angles, etc.) as functions of Weber numbers and Reynolds numbers. This conclusion will also include a brief 1-D model of the drop's oscillation as the surface curvatures variation.

2 Experimental setting and testing conditions.

In this chapter, we will briefly discuss the basic experimental setting of research, including the selection of liquid, and solid material, environmental conditions, and impact controls.

2.1 Testing platform

The parameter selection is based on optical observation by high-speed imaging. A high-speed camera is used to capture the details of the impact process, the FPS is settled to be 2500, and the image resolution is 240 x 240, which is capable of measuring critical information such as dynamic contact angle and spreading diameters. LED provides the light source of backlight image shooting with a brightness of 1200 lux.

A syringe pump provides a fixed flow rate for drop generation. A syringe needle generates droplets for this study. The outer diameter of the needle is 130 micrometers, and the needle's tip is perpendicular to the ground. Since the droplets are creature by gravity, the size of the drop is determined by the liquid's surface tension and the needle's outer diameter. The impact velocities can be controlled by the distance between the needle's tip and the test surface.

It is worth noticing that due to the angle of view, the camera shooting can only capture the droplet's shadowgraphs without observing the asymmetric oscillation on the perpendicular axis, so the droplet's size/average diameter estimation will always have an error of around 2% to 5% percentage.

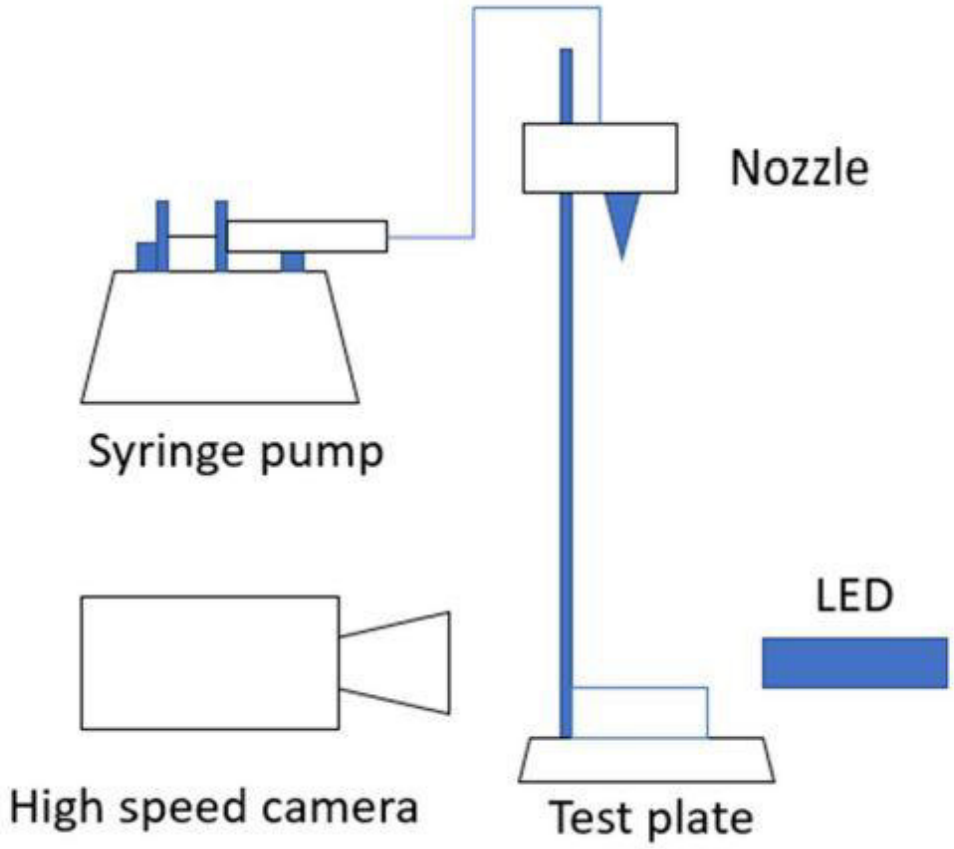

Figure 5.Test platform of droplet impact experiments

2.2 Liquid Selection

To examine the influence of surface tension on impact dynamics, we created multiple components of a mixture for study. Those liquids are based on Deionized water, with a mix of n-propanol under different volume percentages.

Table 2. Selected liquid and solid surfaces for the dynamic impact study

Drop size(mm)	RainX Glass	PTFE	ETFE	Kapton	Glass
Deionized	2.05	2.06	2.09	2.05	2.06

water					
Water + 3% propanol	1.944	1.94	1.946		
water + 5% propanol	1.8	1.81	1.8		
water + 10% propanol	2.03	2.03			
water + 15% propanol		1.56			
water + 20% propanol		1.44			

There are functions to calculate both viscosity and surface tension of mixture liquids. Gambill‘s method is the most widely used function to calculate the viscosity of two liquids’ mixture:

$$\nu_{mix}^{\frac{1}{3}} = x_a \nu_a^{\frac{1}{3}} + x_b \nu_b^{\frac{1}{3}}$$

Due to the high molecular weight of n-propane alcohol, the mixture viscosity is slightly different from the DI water for all these selected fractions. The measurement of viscosities also shows negligible differences. As a result, viscosity is not studied as the primary parameter.

Table 3. Viscosity variation of binary mixture liquids

the volume fraction	0	0.03	0.05	0.1	0.15	0.2

of n-propanol						
solution of water	1	0.97	0.95	0.9	0.85	0.8
the viscosity of the binary mixture	1.002	1.009	1.014	1.026	1.040	1.056

However, the surface tension's mixture variation shows dramatic change via alcohol fraction increases. According to Chunxi's research, the surface tension of a binary mixture can be calculated by the following equation:

$$\sigma = \frac{x_1\sigma_1}{x_1 + f_{12}x_2} + \frac{x_2\sigma_2}{x_2 + f_{21}x_1} - \frac{x_1x_2|\sigma_1 - \sigma_2|}{(x_1 + f_{12}x_2)(x_2 + f_{21}x_1)}$$

Here function f is the factor of binary mixing. According to the calculation, the surface tension of alcohol solutions varies, as the table shows:

Table 4. Surface tensions of alcohol mixture of water

surface tension (N/m)	DI	3% vol propanol	5% vol propanol	10% vol propanol	15% vol propanol	20% vol propanol
	0.072	0.056	0.038	0.036	0.035	0.033

This calculation is proved by the experimental measurement from a tensiometer, the surface tension of mixture liquid has a dramatic effect of change at a volume fraction of 5%, which is also mentioned in the previous study.

2.3 Testing solid substrates

One critical parameter to impact dynamics is the surface wettability; therefore, the section of solid material shall mix the requirements of diversified surface conditions. Based on the surface energy regime, the solid materials are chosen from the hydrophilic, high surface energy materials such as glass to the low surface energy, hydrophobic material like PTFE or ePTFE.

Table 5. The surface energy of different testing solid

surface energy (mJ/m^2)	RainX Glass	PTFE	ETFE	Kapton	Glass
	21~22	18~19	20	48~50	250~500

The variation of surface energy can be presented by the different contact angles of the same type of liquid. Theoretically, the equilibrium contact angle should be constant for one specific kind of liquid on a particular material solid substrate. However, the test results show that the impact velocities influence it. Especially on a hydrophilic surface, such as Kapton. Such phenomenon is potentially related to the wetting accumulation on the solid surface or the impact kinetic energy has to enhance the wetting during the spreading.

Table 6. Impact velocities and contact angles of testing conditions

Material	Liquid	velocity	CA
Glass	DI	0.43	45
ETFE	DI	0.99	97
PTFE	DI	0.43	101
PTFE	DI	0.63	99
PTFE	DI	0.73	100
PTFE	DI	0.794	100
PTFE	DI	0.87	106
PTFE	DI	0.94	102
Kapton	DI	0.35	74
Kapton	DI	0.81	60
Kapton	DI	1.06	55
Kapton	DI	1.29	49

3 Spreading and oscillation of single droplet impacting on a solid substrate

3.1 Introduction

The physics of droplet behavior on a solid substrate, especially the impact and deposition mechanism, is one of the widespread interest topics of microfluidic research. This phenomenon has been widely applied in various industrial fields, including fast 3D printing[68], semiconductive manufacturing[69], internal combustion engine [70], microchannel heat exchanger designing & optimization[71], superhydrophobic coating[72] and micro fabrications[73, 74]. For the study of such complicated multi-phase and multi-scale physics, the experimental investigation is irreplaceable[75].

The droplet impact process can be divided into four phases:1) the kinematic phase which is the initial contact between liquid and solid,2) the spreading phase where the contact diameter continuously increases to the maximum, 3) the oscillation and relaxation phase when the droplet collapses, bounces or quickly stabilizes, depending on the wettability of the solid substrate with the deposited liquid, and finally 4) the wetting/equilibrium phase when the droplet geometry becomes relatively stable and the interfacial tension of the system reaches equilibrium[76]. The time scale of the process varies from microseconds (kinematic phase) to second (wetting phase). One way to study the detailed mechanism of the droplet behavior is to analyse the energy conversion between surface energy and kinetic energy[77]

There are multiple dimensionless numbers to be considered for the study of droplet motion. The one most frequently used is Weber number ($We = \rho D v^2/\sigma$) which is defined as the ratio between the droplet inertia and the surface tension. Here ρ in the liquid density, D the droplet diameter, v the velocity, and σ the surface tension. Another dimensionless number that helps to reveal the dynamics is Reynolds number ($Re = \rho v D/\mu$) defined as the ratio between inertia and the liquid viscosity μ. To characterize the geometric conditions of droplet, the capillary number ($Ca = \mu v/\sigma$) is considered. For high viscosity conditions, or in the relaxation phase, the Ohnesorge number ($Oh = \sqrt{We}/Re$) is the critical scale[32].

In the kinematic phase, the initial contact between the liquid and solid surface makes the contact angle change rapidly. Initial spreading speed of the contact diameter is mathematically a singularity[78]. From the physical point of view, a microscopic mechanism such as Van der Waals force plays as the primary force to drive the expansion[79]. The surface roughness, the air bubble trapped beneath the drop[80], as well as surface temperature all influence the mechanism.

In the second phase (spreading phase), as the contact radius of the droplet continuously increases, the edge of the contact surface forms a wall with an advancing contact angle. This phenomenon commonly appears in hydrophobic surface conditions, and as a result, the "wall" structure will change its shape into a ring structure. Research reveals a vortex formed in this ring structure[15], which absorbs more and more liquid from the center of the drop, and the ring structure continuously develops until the whole droplet expansion reaches the maximum. Introducing the spread factor $\beta = D \ / \ $ where D is

the droplet diameter in the spreading phase and d_0 is the droplet diameter before contacting the substrate, a parameter of interest in this phase is the maximum spread factor $\beta_{\max}$ which is defined as

$$\beta_{\max} = D_{\max}/d_0$$

where $D_{\max}$ is the maximum value of the spread diameter. Researchers proposed various explanations of this parameter. Eggers et al. [78]proposed the maximum spread diameter as a function of Weber number $\beta_{max} \propto We^{0.5}$. Bartolo et al.[81] found that in other conditions it can be fitted as $\beta_{max} \propto We^{0.25}$. Other variables include contact angle[47] and even Reynolds number[82]. This is the parameter directly related to the printing quality[83].

After the maximized spread the phase shifts to oscillation/relaxation where the expansion stops and the whole drop may start to rebounce[19]. This phenomenon varies dramatically with various parameters, especially on hydrophobic or even superhydrophobic surface. The drop typically has a relatively long (compared to the duration of kinematic and spreading phase) period of oscillation. On a superhydrophobic surface the droplet may fully or partially bounce[84], satellite drops may separate from the primary drop and jet into the air or attached beneath the main body which has jumped into the air. There may be the cycle of the regime on the superhydrophobic surface in which non-bouncing, complete bouncing, partial bouncing, and again the non-bouncing regimes. To characterize this phase previous researchers introduced several geometric parameters such as flatness and maximum spread factor[85]. Since this phase has a much longer duration than the kinematic and spreading phases,

the computational research about this phase is relatively rare, and therefore, the studies have been done mainly by experiments.

Finally, after the droplet's oscillation is complete, parameters such as the contact angle and spread diameter are stable, yet slow molecular movement such as peculation and wetting still work[86], which can change the surface conditions after each impact. This is one of the potential reasons for lack of repeatability in our measurements as described later.

Our research focuses on the oscillation/relaxation phase. We are particularly interested in the similarity between two kinds of oscillators: geometry of liquid drop and spring-dumper system. By testing different kinds of liquid on various solid substrates (with different wettability) under various impacting velocities, we measured the geometrical characteristics such ad spreading diameter, droplet height, and contact angle, and tracked their changes as a function of time. By analyzing them, we identified the variables that characterize those geometrical changes, such as decaying constant and oscillation frequencies. We built a model of these variables as functions of Weber numbers and contact angles. Finally, we discussed how the impact velocity can change the duration of oscillation phase, which may help improve the printing speed in applications. This paper mainly focuses on the decaying of spread diameter Other parameters, such as frequencies, will be discussed elsewhere as the future work.

3.2 Experiments

3.2.1 Experimental setup

The droplet is generated using a stainless-steel capillary with a 0.05mm inner diameter. Test liquid is provided to the capillary by a syringe pump and detached as a droplet from the capillary tip by gravity. The velocity of the droplet at the surface impact is controlled by the distance between the tip and the impact surface.

A high-speed camera (Photron FASTCAM-1024PCI) is used with 1800 FPS, 320x320 pixels, and 50 μs exposure time to shoot the images. The backlighting method uses a 1200 lumens tactic flash as the light source.

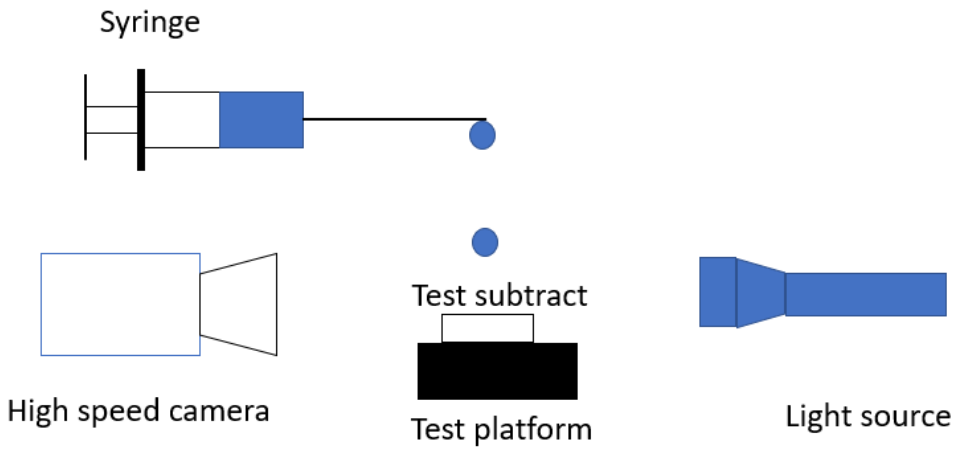

Figure 6.Initial experiment devices of drop impact

For each test, the video recording is triggered manually when the droplet is close to detaching from the tip. The camera resolution limits measurement accuracy. The maximum uncertainty occurred in the manual measurement of drop in air, diameter and velocity have a standard error of 1.8%. Due to the brightness limitation, no diffuser or filter is used in front of the light source. This causes a significant problem in the

background. Therefore, we apply the differential post-process to the raw images before analyzing their images.

3.2.2 Test conditions

Test conditions, including the physical properties of the tested liquids, impacting solid surfaces, some characteristic dimensions of the droplet on the surface, and calculated dimensionless numbers, are listed in Table 7. In this study pure deionized (DI) water and the mixture of deionized water and n-propanol with different volume fraction (from 12 vol.% to 50vol.%) are tested. In order to see the effect of surface wettability, five different materials are used as the solid substrate with pure DI water and two materials for the mixture. The static contact angle for each liquid-surface combination is measured with the sessile drop measurement. Maximum spread factor defined as $\beta = D_{\max}/d_0$ and steady flatness defined as $\delta = h/d_0$ where $D_{\max}$ is the drop diameter at maximum on the surface, d_0 is the drop diameter prior to impact, and h is the drop height, are determined from the captured images. Surface tension is measured using the Wilhelmy method. Finally, the Reynolds number and Weber number are calculated using the above properties, and the droplet speed is obtained with two successive images just before the impact on the surface.

Table 7.Liquids applied in experiments

liquid	surface tension(N/m)	Viscosity (mPa*s)	Density (kg/m^3)	Re	We
DI water	0.072	1.002	1000	14159±510	300±16
12%n-propane	0.0356	1.024	977	14514±522	419±23
16%n-propane	0.0315	1.032	968.5	12771±460	419±23
20%n-propane	0.0286	1.041	960.6	13074±470	475±26
30%n-propane	0.0281	1.067	940.6	12893±464	492±27
50%n-propane	0.02558	1.141	901	12230±440	545±30

Table 8. Test conditions and critical parameters on different solid substrates

liquid	surface	steady contact angle (°)	maximum spread factor	steady flatness
DI water	ETFE	84	2.33	0.42
	PTFE	94	1.95	0.292
	Kapton	34.7	2.6	0.35
	Aluminum	21.4	1.71	0.185
	Acrylic	30	1.89	0.26
12%n-propane	ETFE	90	2.76	0.478
	Kapton	21.4	2.13	0.184
50%n-propane	ETFE	21.5	1.925	0.184

3.3 Results and Discussion

3.1 Oscillation of water droplet flatness

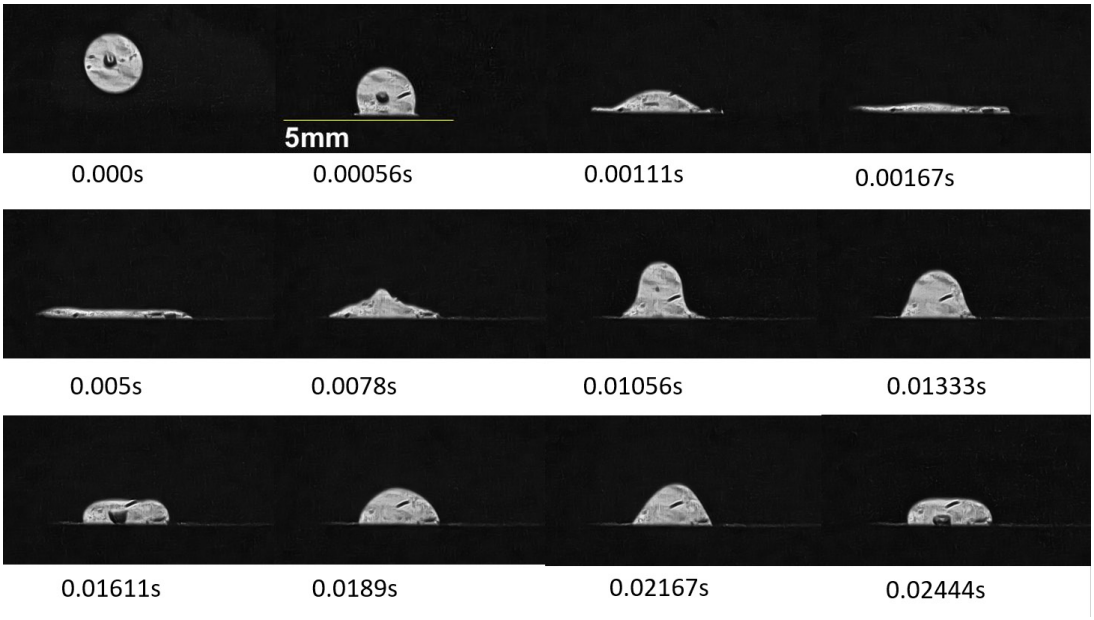

Figure 7.DI water droplet's impact and spreading phases on ETFE surface. Original images have been processed with MATLAB code to track the droplet's shape

The spreading and relaxation phases of the hydrophobic surface show more similarities to the typical damped harmonic oscillation (DHO) model, which can be described as

$$X(t) = X_{eq} + Amp_{beta} e^{(-Bt)} \cos(\omega t + \phi) \quad (1)$$

Here $X(t)$ can be various geometric parameters, such as flatness which is defined as the droplet height over the spread diameter

$$\delta = H_{drop}/D_{spread} \quad (2)$$

And X_{eq} is the value at the equilibrium condition which typically is constant.

Flatness is the primary parameter to be examined and analyzed because it is sensitive to the oscillation frequencies.

However, the flatness is difficult to measure for high-velocity conditions. Thus, the spreading factor can be selected as the primary parameter:

$$\beta = D_{spread}/D_0 \quad (3)$$

where the D_0 is the diameter of droplet just before impacting the substrate.

Figure 8 shows the change of droplet flatness with time for the first case in Table 1 (DI water on ETFE surface). The difference between the DHO model and real data is significant at the beginning of the process. The first peak predicted by the model has a significantly greater amplitude compared to the measurement. After the first peak, the model agrees well with the experiment.

The discrepancy of initial peak predicted by the model from the measured data varies depending on the liquid properties. Only the first peak of impact for DI water shows a clear difference as seen in Figure 1. In the case of the DI water/n-propyl alcohol mixture, drop flatness is more unstable, and the peaks are not clear at the early stage.

Figure 9 shows the flatness change of a DI water droplet on the hydrophilic surface. On a hydrophilic surface, unlike the hydrophobic one, surface tension overwhelms the inertia, and the oscillation curve damps faster.

Equilibrium spread diameter is determined by the surface wettability, while maximum spread diameter is primarily controlled by the kinetic energy of the droplet motion.

Higher wettability leads to faster energy conversion from kinetic to interfacial. The surface comparison reveals the influence of interfacial tension on the damped coefficient and equilibrium condition.

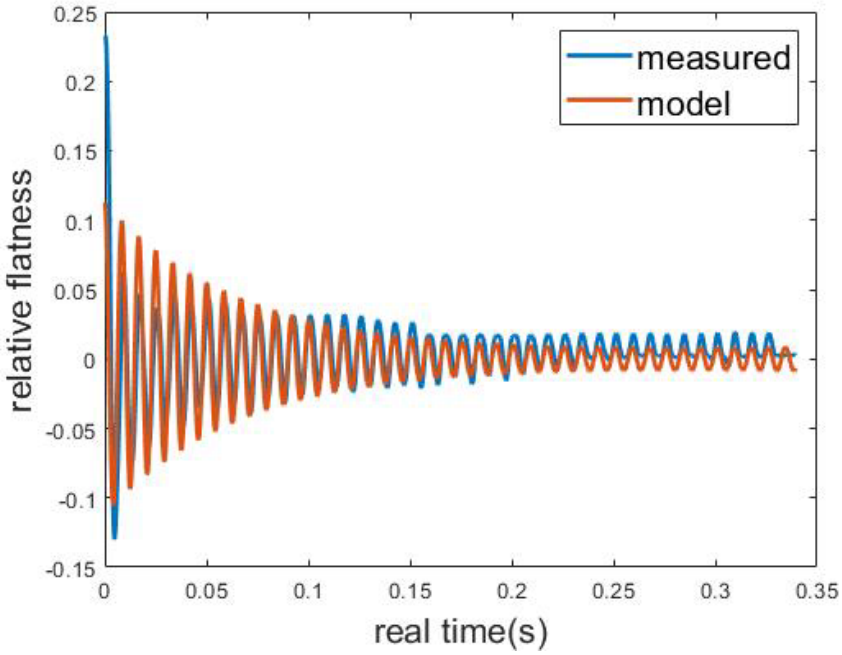

Figure 8. DI water droplet post-impact oscillation on ETFE surface. The model curve is represented as a function of the second-order coefficient damped harmonic oscillator (DHO).

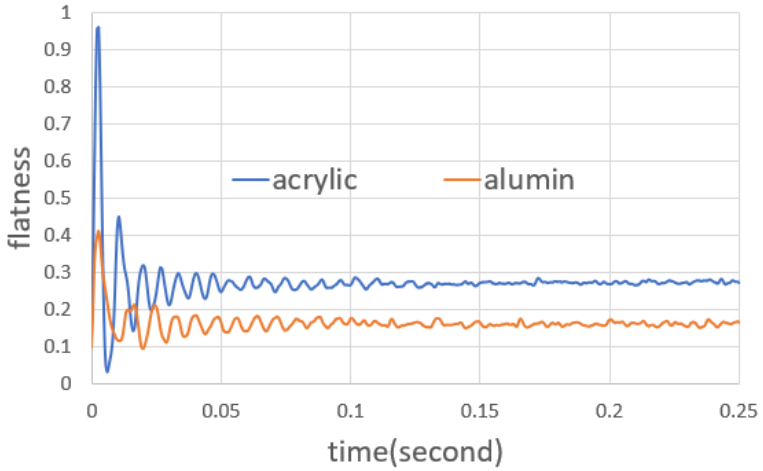

Figure 9. DI water droplet post impact oscillation on acrylic and aluminium surfaces. Compared to the ETFE surface in Figure 3, the damped coefficient is significantly higher for these two cases.

3.3.1 Proposed model with two-term oscillation amplitude and damped coefficient

The mixture of n-propyl alcohol and DI water has different surface tension and viscosity values. As a result, the oscillation profile significantly differs from the typical DHO,especially for the spreading factor measurement. Spreading diameter reduction is too fast to be fitted by a single-term exponential function at low velocity / high surface tension conditions as shown in Figure 10.

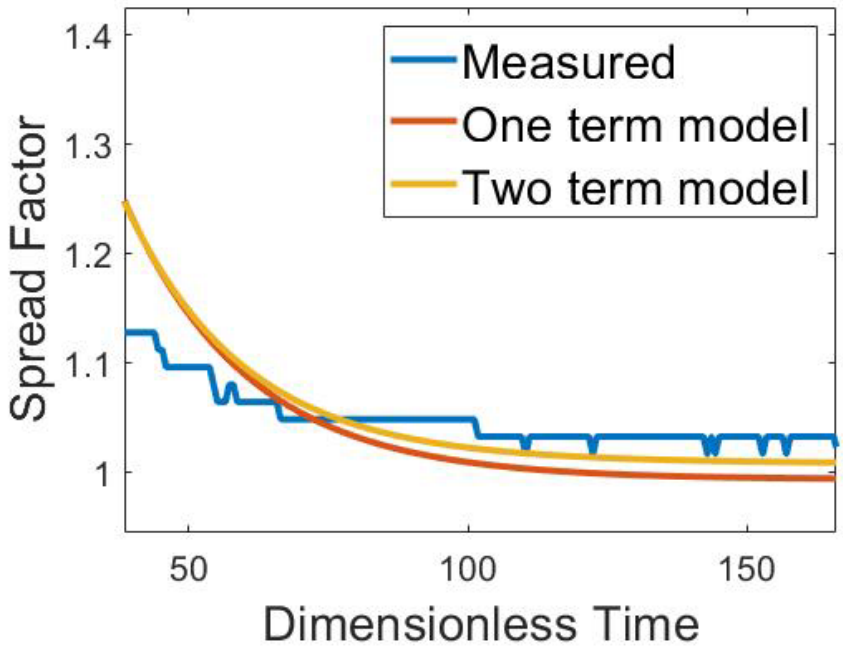

Figure 10. The spread factor of Pure DI water impact on ETFE surface, with a velocity of 3.45 m/s. Noticed that the model created by single term function has different ending conditions from the raw data

To improve the accuracy of the mixture oscillation model, we replace the "equilibrium" term $X_{eq,}$ which was constant in our original model in equation 1, with the dynamic exponential function.

$$X_{eq} = X_{eq}(t) = X_{wetting}e^{-\lambda_{wetting}t} + X_{stable}e^{-\lambda_{stable}t} \quad (4)$$

This function represents the process that dynamic equilibrium approaches the final steady state. Factor $X_{wetting}$ is described as the amplitude influenced by a solid surface wettability, and X_{stable} is the final state equilibrium variation, while $\lambda_{wetting}$ and λ_{stable} are the damped coefficients of these two terms. This also reveals a potential mechanism that the equilibrium is not a steady state but a decaying process.

Depending on the damping precision requirements, the oscillation amplitude Xeq (t) can be simulated by either single term or two terms. The two-term oscillation model damped slower than the single-term model, as shown in Figure 10.

Therefore, the whole equation of geometrical parameter oscillation becomes

$$X(t) = \left(X_{wetting}e^{-\lambda_{wetting}t} + X_{stable}e^{-\lambda_{stable}t}\right) + Amp_{beta}e^{(-Bt)}\cos(\omega t + \phi)\cos(\omega t + \phi) \quad (5)$$

where both factors λ_{stable} and X plays critical roles in droplets shape-shifting, yet $\lambda_{wetting}$is close to zero. As the liquid surface tension further decreases, oscillation of the flatness trends to negligible, as Figure 6 shows.

For different liquid mixtures , change of surface tension influences the final equilibrium state and the oscillation process.

This modified function can be interpreted as a mechanism that the diameter collapsed faster at the beginning of the relaxation phase and then stabilized by the contact area limitation.

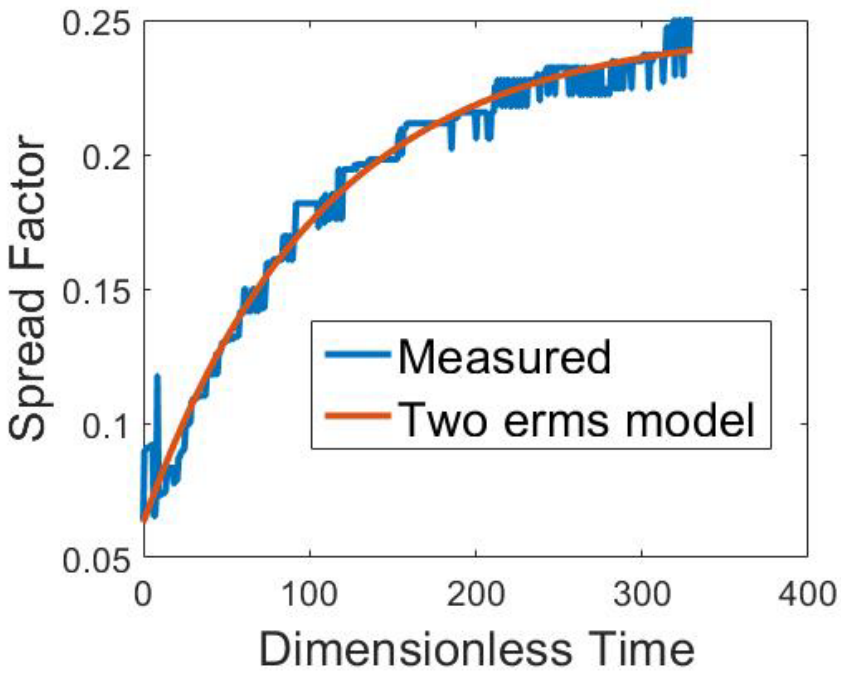

Figure 11. Experimental data and model of droplet oscillation on ETFE surface when the liquid solution is Di water with n-propyl alcohol (vol20%). Oscillation becomes underdamped in this case.

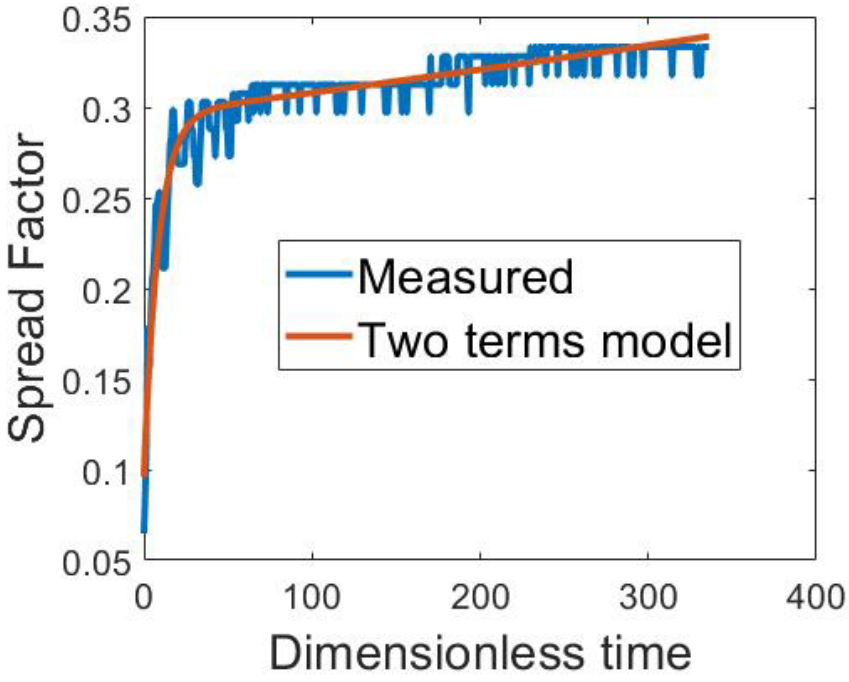

Figure 12. Pure DI water droplet on ETFE surface, noticed the curve has sharper bending shape compared to the hydrophilic surface

3.3.2 Oscillation parameters as functions of We number and Contact angle

Since the droplet shape is determined by the surface tension and the substrate wettability, it is sensible that the equilibrium state derived from the oscillation function should be a function of Weber number. During the oscillation, on the other hand, the kinetic energy is mainly absorbed by viscosity, and therefore the damping coefficients of the model can be described as functions of Re number.

Analysis results show that the droplet maximum spread factor changed linearly with both We and Contact Angle. As we compared the oscillation results from different

liquid solutions, the oscillation parameters (maximum spread factor) from eq.4 can be described by the following functions

$$\beta_{max} = -0.019We + 12.7 \quad (6)$$

$$X \cong 0.71$$

$$\lambda_{stable} = -3135.5\exp(-0.008We) \quad (7)$$

$$\lambda_{wetting} = 0.000071We^{0.25} \quad (8)$$

or in terms of the contact angle,

$$\beta_{max} = 0.064CA - 0.7897 \quad (9)$$

$$X \cong 0.67$$

$$\lambda_{stable} = 12.46\exp(0.0226CA) \quad (10)$$

$$\lambda_{wetting} = 0.0000054We^{0.3} \quad (11)$$

From the equations above, we can make assumptions that the surface tension decreases dramatically when the n-propanol volume fraction increases, as well as the decaying constant increases .

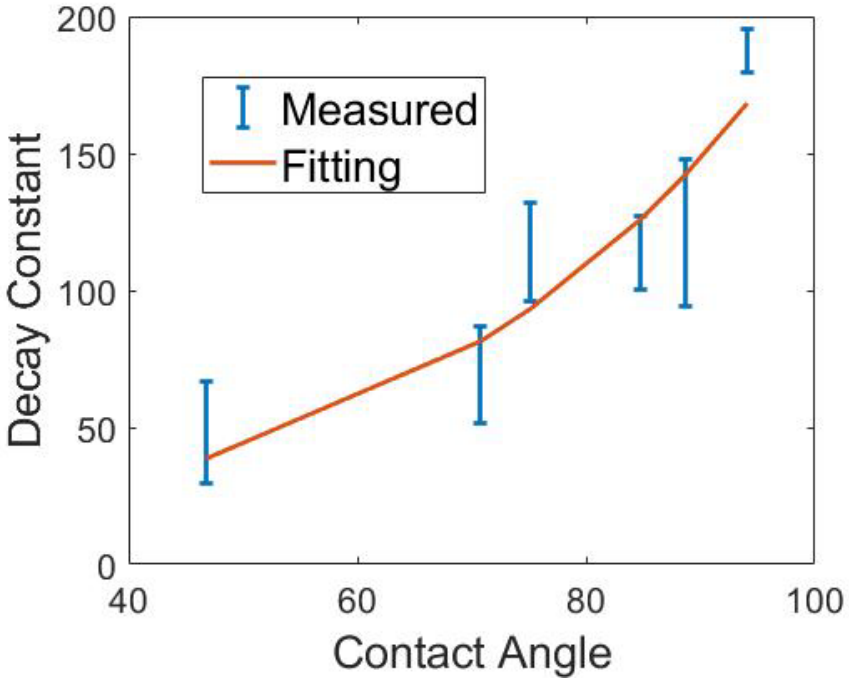

Figure 1312. dynamic equilibrium flatness' amplitude as a third order polynomial function of Contact number

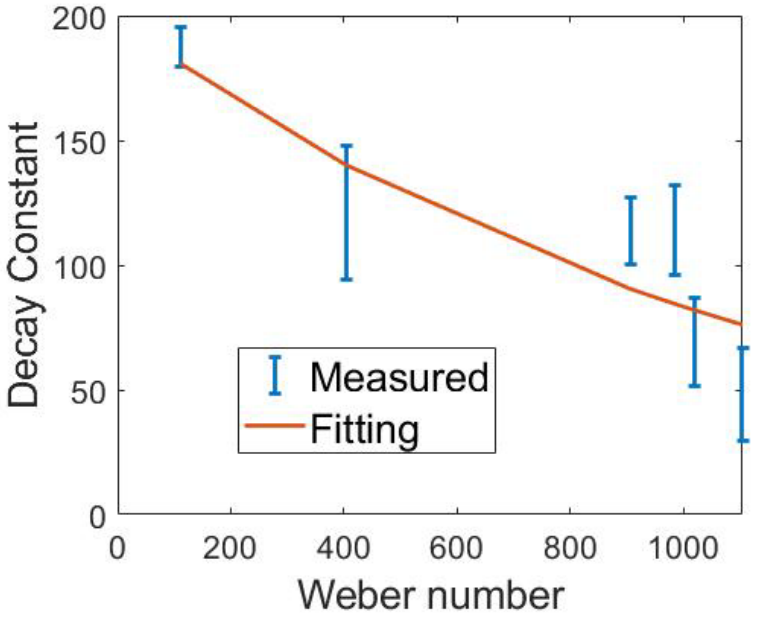

Figure 14. decay constant of diameter as a function of Weber number

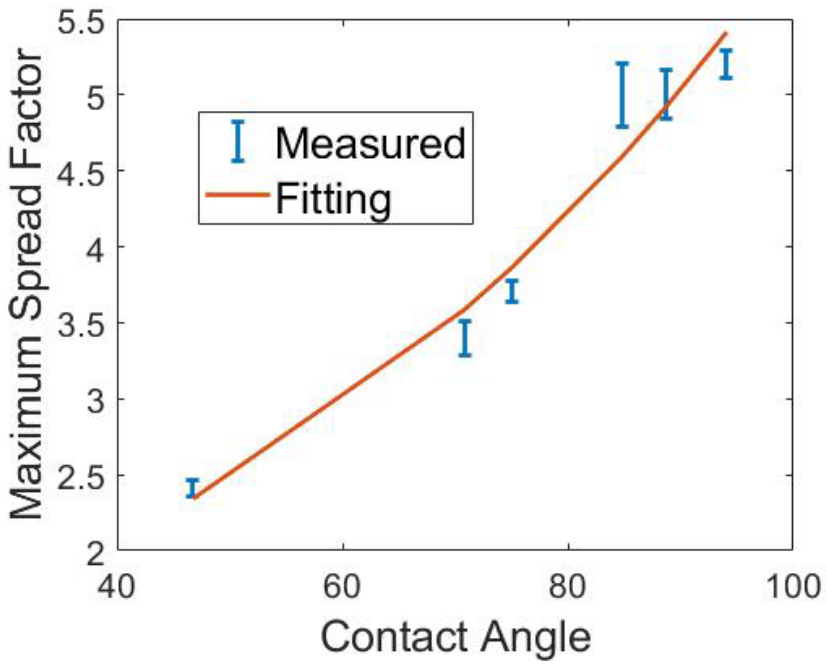

Figure 13. droplet's maximum spread factor as a function of contact angle

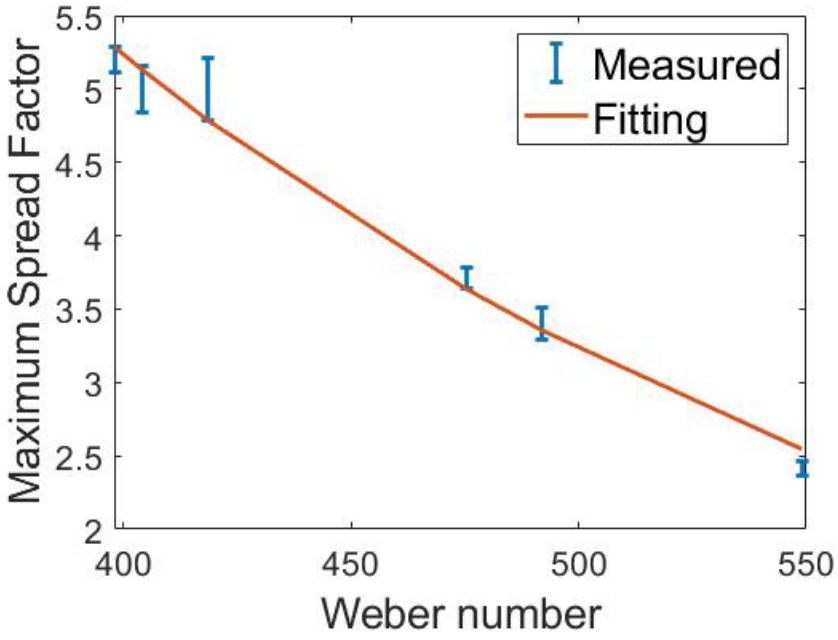

Figure 146. droplet's maximum spread factor as a function of weber number

3.4 Conclusion of this section

In this research, we analyzed the droplet impact and post-impact phases, exploring the limits of the typical DHO model on the droplet's impact mechanism. To expand the applicable range of DHO, the equilibrium condition should be considered a dynamic component as a function of time instead of a constant. Furthermore, the two-term amplitude model can improve the model's accuracy from the single-term model at the wetting/spreading phase. Due to the limitation of test conditions, unfortunately, our study on implementing the effect of other parameters such as Re, We, and contact angles into our model, as well as the mechanism of oscillation frequencies exploration, are still in process, primarily because of the lack of reliable data sets, especially in the critical area, and remains for our future task.

4 Oscillation dynamic of droplet impact on solid substrate: frequencies issue, and satellite drop separation.

4.1 Introduction

Droplet impact dynamic is one of the popular subjects of microflow research, the widespread application of this dynamic can be found in multiple industrial or engineering topics, including aircraft icing[87], direct injection combustion engines[15, 16, 19], thermal spray processing[1-3], spray cooling[88], ink-jet printing[71, 83] and microfluid technologies[71, 74].

There are multiple parameters used in these dynamics, based on the energy conversation between kinematic, surface energy, and viscosity consumption, the most critical variables include the Weber number, which describes the ratio of drops' inertial over surface tension; Reynolds number, which can be revealed as the inertia versus viscosity; and bond number, which is the ratio of weight over surface tension. The process takes a short time (mainly microsecond scale) in a low Reynolds number (due to the millimeter or even micrometer dimension).

In practically, the whole process can be separated into four steps or phases: The kinematic phase, in which the drop initially contacts the solid surface; spreading phase, in which the drop's contact diameter continually increases to maximum; relaxation phase, in which the drop's diameter starts to receding and the shape oscillated for a while; and equilibrium phase, which the condition of the drop is approaching to

equilibrium states, and shape-shifting is negligible and only driven by peculation in relatively long term[76].

At the kinematic phase, the initial contact is driven by kinetic energy, the van de Waals force[79], and surface tension. Although the contact diameter's initial spreading velocity is

Uneasy to be estimated (because it is mathematically a singularity); in practice, the surface's roughness, the air bubble trapped beneath the drop[79], and the fluctuation of the surface will influence the results.

The most exciting topic of the drop impact is the dynamics of the second phase, especially the condition at maximum spreading diameter. The drop at the advancing process can form a "wall" around the main body, which will finally become a torus ring structure. Based on different impact velocities, the structure's shape changed from the regular ring, corona splashing, to receding splashing [39]. former research reveals that vortexes will occur in the ring, which absorbs the kinetic energy from impact by viscosity[89]. The most focused parameter in this phase is the maximum spreading factor, which is defined as:

$$\beta_{max} = \frac{D_{max}}{D_{drop}}$$

This parameter relates to industrial applications, including ink jet printing and thermal spray. Researches on this subject contain several mathematical models from different input variables, for example, the spreading factor as a function of Reynolds number[45]($\beta_{max} = \sqrt{\frac{4}{3} Re^{\frac{1}{4}}}$),or complicated equations of weber number, Reynolds

number and contact angle(both equilibrium and advancing contact angle). Chandra and Avedisian[44] provide a functions as a 4th order polynomial function of β_{max}, with factor Weber number ,Reynolds number and contact angle; other researches also provide function of polynomials with those three parameters[43, 46, 47]. Such diversified models are based on different approaching tactics of the similar phenomenon.

After the maximum spreading, the rebounding/relaxation phase is also the hot topic of the impact study. Rebounding mainly occurs in hydrophobic or even super hydrophobic cases. During the stage, the ring structure starts to collapse with rotations[90], which may cause the asymmetricity [64] of the shape and further enhance the droplet's surface mean curvatures. Hence, the process of this phase is complicated and more challenging to be modified. Also noticed, the bouncing on the superhydrophobic surfaces can be either fully or partially, depending on the impact velocity[84]. It is also interesting that the drop's shape relaxation may be similar to the harmonic oscillator; therefore, studying oscillation characteristics, such as the frequencies and damped ratio[85] is also recommendable for analyzing these mechanisms.

Finally, after the relaxation of the drop's shape is fully damped, the form of the drop on the solid surface will change slowly by evaporation or percolation; this is the last phase of the equilibrium[86]. Such dynamics may also change the surface's wettability, making the post-impact contact angle measurement unstable.

Our research mainly focuses on the third phase by applying the modified damped harmonic oscillator model to the drop's shape relaxation and analyzing the roles of

weber number and solid surface energy. Also, the rebounding on hydrophobic surfaces will be discussed, especially the mechanism of satellite drop separation and jetting.

4.2 Experimental setting

This study's experimental setup is based on the high-speed camera imaging of drop deposition. A camera with 2500 fps is mounted on the table with a microscopic lens. Thanks to the low exposure time (10 microseconds), the images are sharp enough for tracking the drops' movement and spreading. The resolution of the photos is 240 x 240, capable of contact angle measurement, oscillation, and spreading observations. Driven by gravity, droplets generated by syringe needles are perpendicularly deposited on selected horizontal flat solid substrates, so their impact velocity is controlled by changing the height of the needle. A LED flashlight with 1200 lumens provide high enough brightness for backlight image shooting. All the images were shot horizontally. Therefore, the asymmetric splashing/rebounding are not able to be captured. According to the resolution, the error of geometric parameters such as drop's height and spreading diameter is less than 2% of the initial diameter. And the timing error is lower than 10% of the dimensionless time.

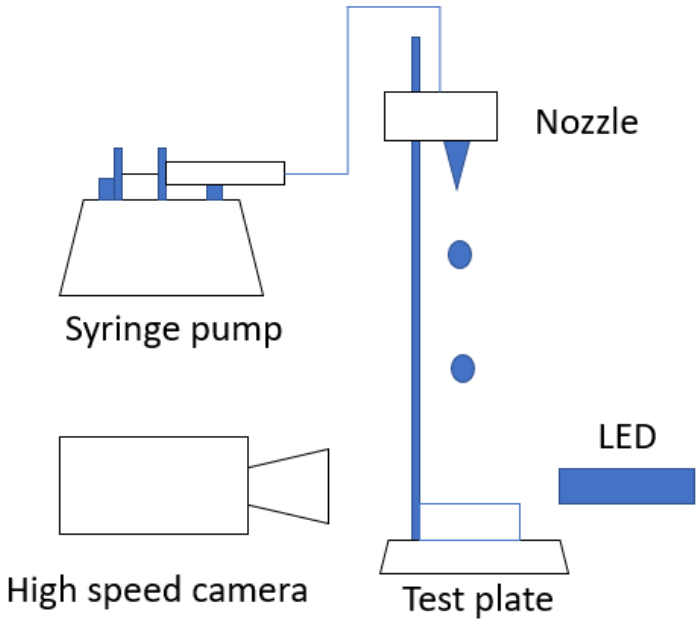

Figure 157. Test platform of droplet impact measurement.

4.3 Test conditions

To analyze the mechanism, the test schedule is focused on a combination of liquid type and solid material and the various impact velocities. Solid substrates including PTFE, ETFE, Kapton, and glass (with and without surface coating by rain X). Most solid materials are hydrophobic for deionized water; this is because drop's behaviors on such low surface energy materials are relatively easy to be observed and measured; besides, by changing the chemical components of the mixture liquid, the wettability of solid can also be adjusted with low energy material such as PTFE.

Liquid components contain deionized water and a mixture of n-propyl alcohol with different fractions. According to the tensiometer measurements, the surface tension of

minutes changes dramatically at low alcohol volume fraction, then changing becomes smooth as the proportion increases. Since the molecular weight of n-propane alcohol is much higher than water, the viscosities of tested components have an insignificant difference. Thus, we do not consider Re a separatable variable in our study.

Table 9. Test matrix of different solid substrate materials and liquid components. Most tests are done on the hydrophobic material.

Drop size(mm)	RainX Glass	PTFE	ETFE	Kapton	Glass
Deionized water	2.05	2.06	2.09	2.05	2.06
Water + 3% propanol	1.944	1.94	1.946		
water + 5% propanol	1.8	1.81	1.8		
water + 10% propanol	2.03	2.03			
water +		1.56			

15% propanol					
water + 20% propanol		1.44			

surface energy (mJ/m^2)	RainX Glass	PTFE	ETFE	Kapton	Glass
	21~22	18~19	20	48~50	250~500

Table 10.Surface tension of different liquid components. Notice there's a dramatic change in propanol's volume fraction around 3%

surface tension (N/m)	DI	3% vol propanol	5% vol propanol	10% vol propanol	15% vol propanol	20% vol propanol
	0.072	0.056	0.038	0.036	0.035	0.033

4.4 Results and discussions

4.4.1 Variables that determine the oscillation frequencies

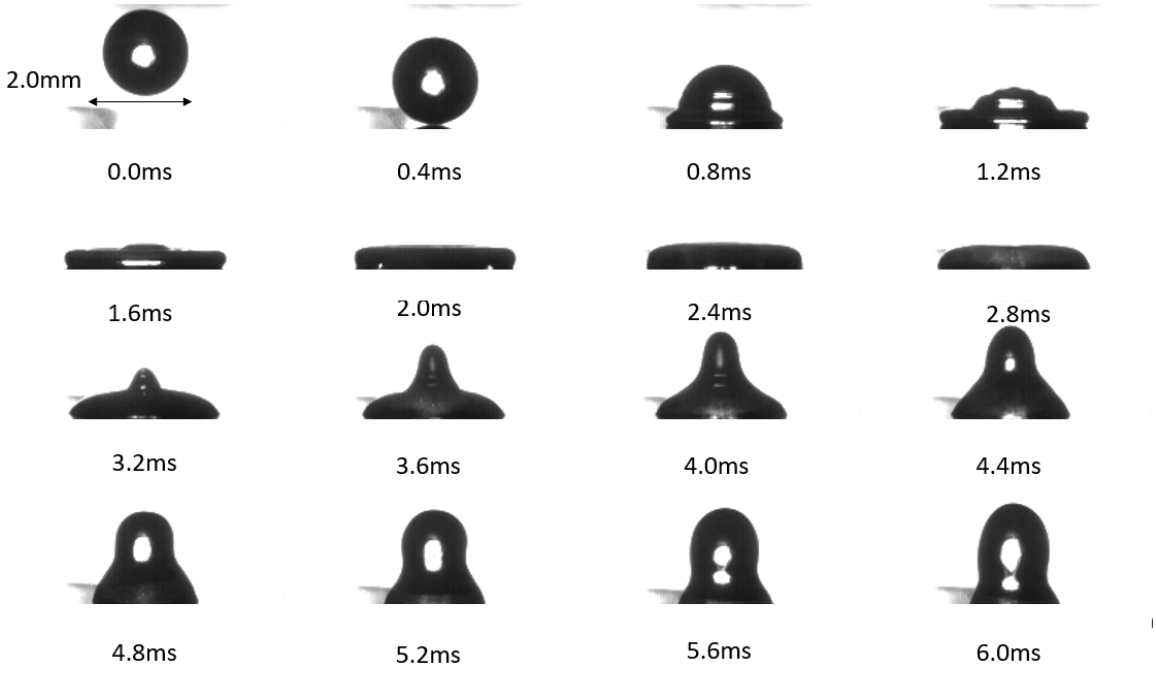

Figure 168.DI water droplet impacts on PTFE surface, with We=26.

Our research starts from the assumption that the droplet's behaviors are highly like the solid spring system. Therefore, the damped harmonic oscillator model can be applied to this problem. In typical DHO, damped frequency ω is the modification of natural frequency $\omega_0$under the influence of constant decay c :

$$\omega = \sqrt{1 - \frac{c^2}{4mk}}\omega_0 = \sqrt{\frac{k}{m} - \frac{c^2}{4m^2}}$$

Where k is the spring stiffness, In solid spring respect, stiffness is the physical property to maintain the spring's stable shape.

Another oscillator model which highly like this research object is the RLC circuit model, in which Induction determines the frequencies, capacity, and resistance, as the equation shows:

$$\omega_0 = \frac{1}{\sqrt{LC}} \qquad \omega = \omega_0\sqrt{1-\zeta^2}$$

Most likely, such a property could be surface tension for liquid droplets. On the other hand, the decay constant is the system's ability to absorb the movement and convert kinetic energy to internal energy. In the liquid's respect, this is highly like viscosity. Since both surface tension and viscosity are properties of liquid that are only determined by component and temperature, for the same kind of liquid and negligible temperature change, the decay constant should be stable as well as the surface tension; therefore, the oscillation frequencies should be independent of various of impact velocity.

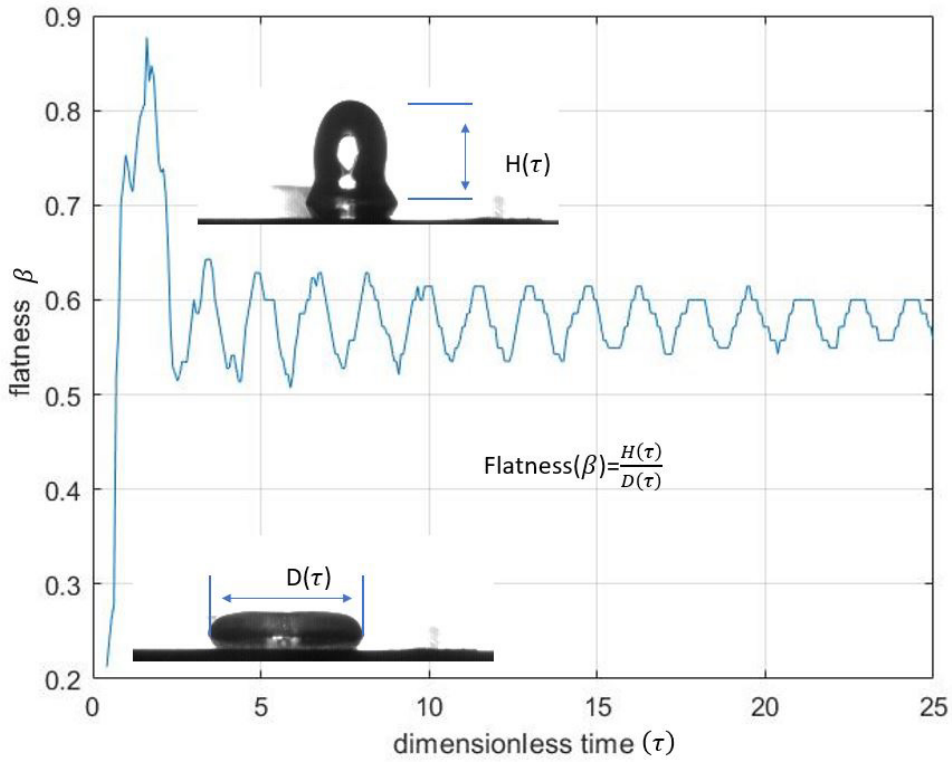

Figure 19. 17Flatness of DI water impact on PTFE change via dimensionless time, with We = 26

However, the tests' results are not highly stable; instead, the oscillation frequencies show influence from multiple parameters: surface energies (for both solid and liquid), interface energy, and impact velocity.

In low bond number conditions, the drop's mass plays a relatively unimportant role compared to the spreading coefficient, especially in pure water drop conditions. The equilibrium contact angle after impact changes via different spreading parameters by changing the substrate's material.

To minimize the variable in this topic, the first selection is pure deionized water conditions and measuring the oscillation frequencies of the droplet's height. According

to the observations, the frequencies vary like a parabolic function, where the oscillation frequencies reach the maximum at hydrophobic conditions, with a contact angle of around 70 degrees. That is when pure water drop is deposited on Kapton, where the surface energy is 50mJ/m^2.Mid-Surface energy material provides higher oscillation frequencies than high or low energy surface.

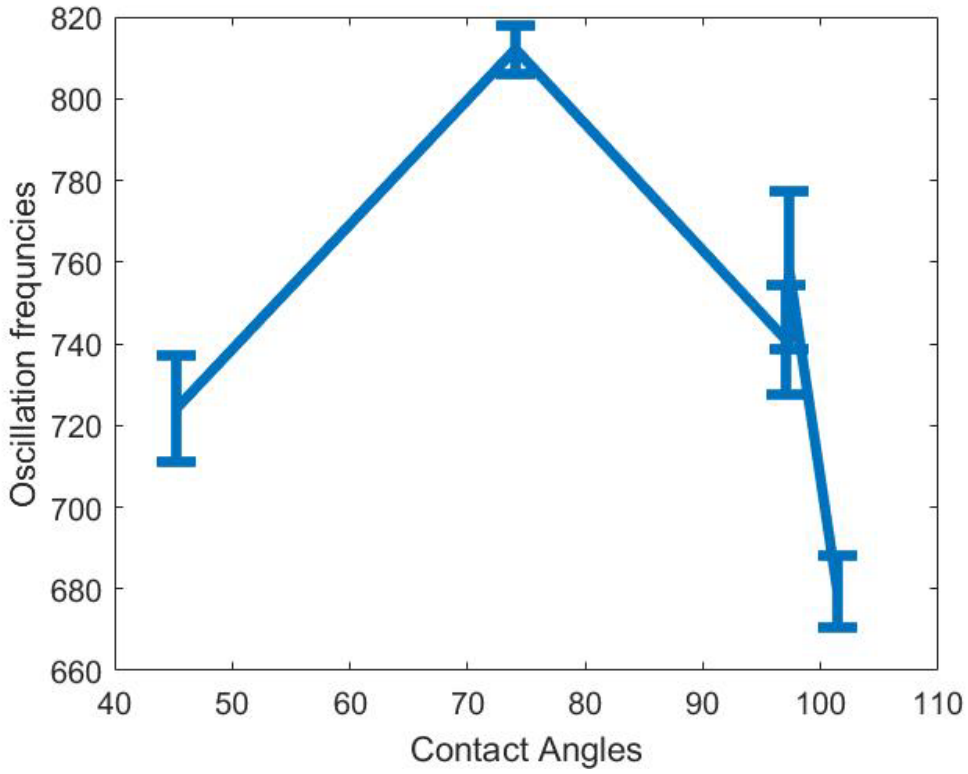

Figure 20. Oscillation frequencies of DI water drop impact on different solid materials, from hydrophilic to hydrophobic

A similar phenomenon also occurs on an additional component of liquids drops on the same solid material. With the same impact velocity, the frequencies valley or peak

located at the percentage where surface tension of the mixture has the most rapid change

Table 11. Drops of different liquids impact PTFE substrate; notice that liquid of I water mixture with 5% volume of propanol has the maximum oscillation frequency

Liquid	Size	SFT	Velocity	rho	We	CA	W	W_std
DI	2.05	0.072	0.94	1	25.16	101.6	703.6	21.95
p03	1.89	0.056	0.94	0.994	29.64	92.15	741	26
p05	1.75	0.038	0.94	0.99	34.02	75.65	767.3	7.9
p10	1.61	0.036	0.94	0.976	39.67	49	720	18.4

One potential explanation is that the spread parameter, which is determined by surface energy and interface energy, plays similarly to the "mass" in the spring oscillator or "capacitor" in an RLC circuit to limit the energy capacity of a system by potential

energy storage. When the solid surface energy is too low, the ability is not enough to store the energy for maintaining oscillation. On the other hand, if the solid surface energy is too high, the higher spreading diameter will flatten the drop and limits the amplitude of oscillation, which also helps the damping. This is especially common in low bound number drops with low impact velocity.

Table 12. Oscillation frequencies of different liquid drops impact on solid substrates with velocity (v = 0.35m/s)

lowest velocity	RainX	PTFE	ETFE	Kapton	Glass
DI	741	704	758	812	724
water + 3% vol propanol	771	741	738		
water + 5% vol propanol	814	767	796		
water + 10% vol propanol	821	720			

Experimental results show that the contact angle after the relaxation changes via velocity, higher impact speed will cause a lower contact angle, and the oscillation frequencies reduce as the velocity increases. For a hydrophilic surface, the oscillation frequency and pseudo-equilibrium contact angle are also changed by the impact velocity, as figure 5 shows. Higher velocity may cause microscopic drops to separate from the main body, wetting the surface around the maximum diameter and changing the wettability of the solid surface.

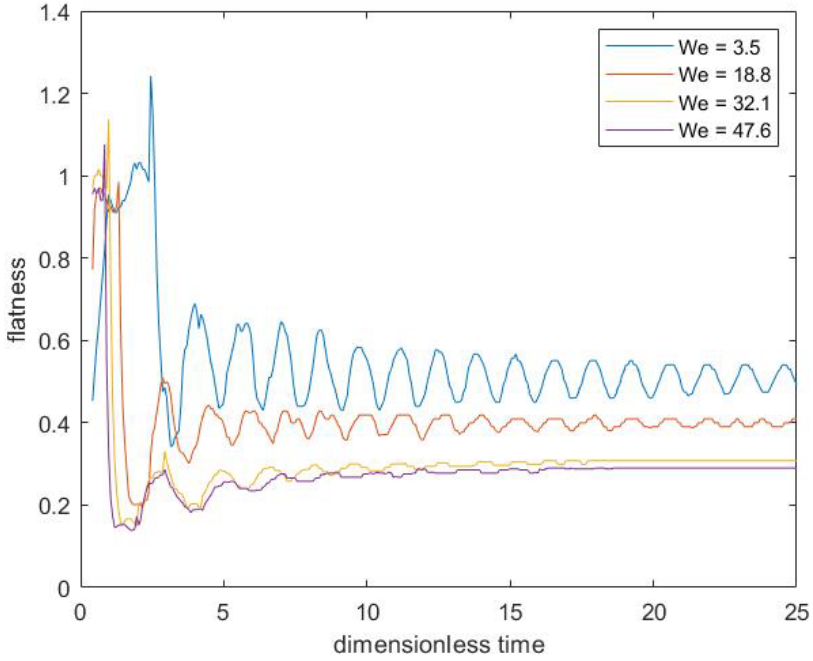

Figure 21. Flatness oscillation by DI drop on Kapton surface, with different Weber number

Details of initial rebound: tip formation, satellite drop separation, and partial rebound

One topic of drops' oscillation is the initial shapeshifting at the relaxation phase and rebounding, especially on hydrophobic or superhydrophobic surfaces. Such a phenomenon also relates to the tip formation at the top of the drop.

After the initial impact, a series of waves of surface flux will occur at the edge of contact as the reflection from the solid surface flows upward. This phenomenon forms the first series of tips at the top.

For a hydrophobic solid surface, a satellite drop will be separated from the main body as a sharp tip formed; instead of reflection waves, the tip is created by the relaxation of the drop's ring structure.

Mechanism of such physics can be explained by surface mean curvature distribution: for hydrophobic or super hydrophobic surface conditions, we focus on the moment when the drop reaches the maximum spreading, there will always be a ring structure formed on edge, as well as the relative flatten "cylinder" at the center of the whole body. At that moment, the top point of the drop will have positive mean curvature, which pulls the top point outward; the outer area of the ring is pushed by the capillary pressure formed by negative mean curvature. These are the initially driven forces of the droplet's rebound. The ring's shape at this moment, the contact angle is almost 180deg, which means the ring torus's bottom is located at the contact surface.

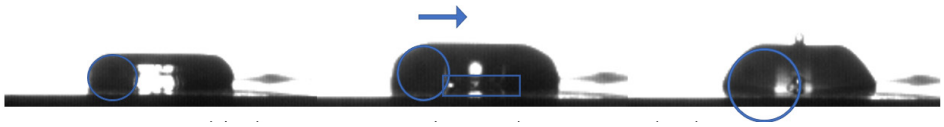

Figure 18 . Droplet re-collapse after the maximum spreading. Noticed that the ring torus structure around the drop has an increasing diameter, as the collapse continues

After that moment, the torus ring starts to collapse inward. Due to the vertex within the ring, liquid beneath the drop surface tends to flow into the ring, which may help the ring's volume to increase further. What happens next should be explained geometrically: if the volume of the ring is big enough, the liquid in the central valley will be absorbed quickly. Therefore, the torus will transform from ring to horn, as figure 6 shows. During the process, the "main body" of this torus is still above the solid surface, so the curvature distribution is similar to what figure x shows; the inner circuit of the torus continually decreases, and as a result, the curvature of it increases rapidly, and finally reach to a mathematical "singularity" when the ring starts to self-intersecting. The sudden increase of capillary pressure will pull the droplet's top upward, and the high gradients of curvature distribution will help it to create a hyperbolic tip, sharp enough to cut off the satellite drop from its narrowest connection.

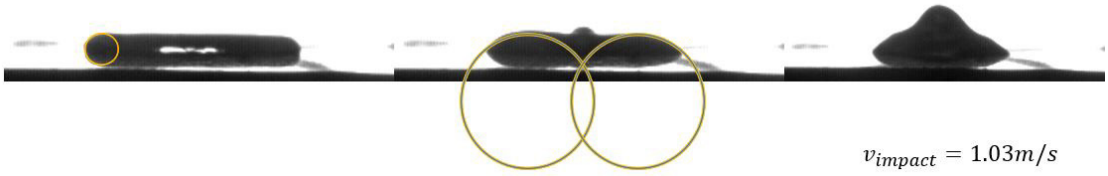

Figure 23. Tip formation failed at high-velocity impact, noticed that the mean curvature of the top is too low for the hyperbolic cone

Figure 24. Satellite droplet separation success at low Weber number condition(left) and failed at high Weber condition(right)

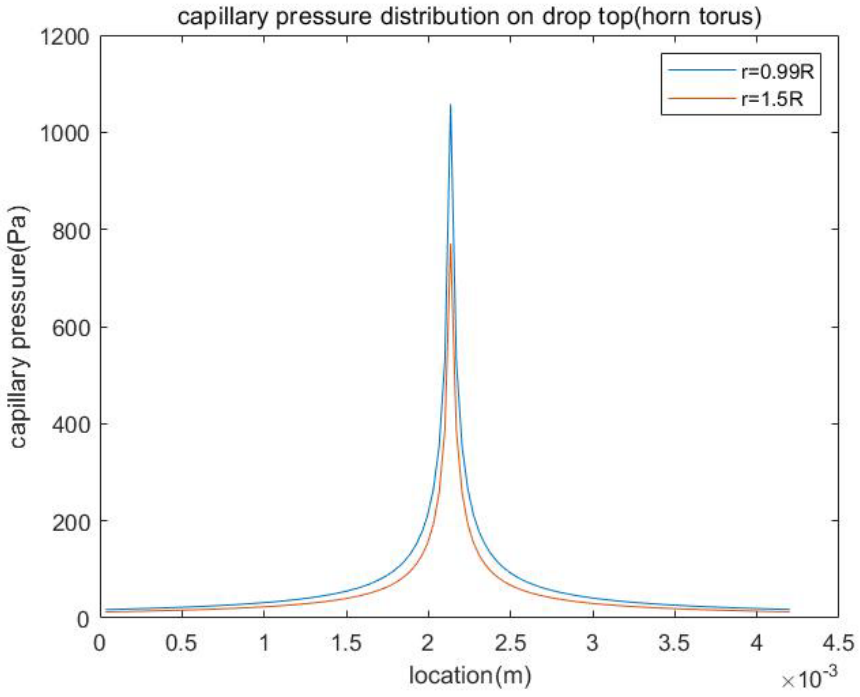

Figure 19Capillary pressure distribution on the drop's top surface when self-intersecting begins. Notice that if the radius of torus from center to tube's axis (known as R) and radius of the tube (known as r) are similar, then the intersection mean curvature is maximized

Whether the tip formation success or not depends on the proportion of ring in the whole drop. According to the measurement, when the ring's proportion is higher than 50%, the

sharp tip will be created; when the proportion is higher than 70% percent, the satellite drop will be detached from the main body. However, suppose the proportion is too low. In that case, the ring's enlargement in collapse will be far slower than its radii increment, so the intersection "singularity" will not occur on the top of the drop. The impact velocity determines the proportion; higher velocity leads to a larger spreading diameter, which pushes the ring outward, reduces its volume, and delays the collapse process.

Table 13. DI water drop's tip formation and satellite drop separation on a hydrophobic surface, as the variation of impact velocity

v(m/s)	Vol fraction (%)	Hyperbolic Tip formed	Satellite drops separated
0.43	78.8	yes	yes
0.73	57.5	yes	no
0.86	45.3	no	no
1.03	35.6	no	no

4.5 Conclusion of this section

By applying tests of multiple liquids on a different solid substrate with various impact velocities, we examine the influence of liquid properties on oscillation dynamics. Unlike the assumption that the oscillation behaviors are only determined by liquid's surface tension as well as solid's surface energy, the impact inertia, which is presented

by the Weber number, also plays a critical role, especially on a hydrophilic surface; this is potentially due to the percolation on a solid surface, higher impact velocities improve the wetting further. Also, we discuss the potential mechanism of satellite drop separation and drop bouncing (fully and partially) on a hydrophobic surface, which is due to the mean curvature change on the drop's top surface. Such phenomenon only occurs at a specific range of Weber numbers with a normal hydrophobic surface. Further studies will focus on viscosities' influence on the impact mechanism and the potential bouncing on superhydrophobic surfaces.

5 Droplet's impact behaviors on a solid surface, viscosity influence, and dynamic contact angle.

5.1 Introduction

The droplet impact on a solid substrate is one of the most typical complicated problems of dynamics and a widely appeared phenomenon in nature and industry. Raindrops dancing on the lotus leaves, the melted metal deposited during the thermal spray, ink from the printer impinged on paper; all those phenomena are within the research range of impact study.

The impact phenomenon is driven by balancing different factors: surface tension, solid's wettability, viscosity, impact velocity, droplet's mass, and volume, and environmental parameters (such as temperature, humidity, etc.). To analyze the dynamics, there are multiple dimensionless parameters: Reynolds number, which describes the ratio between liquid's inertia and viscosity; Weber number, the parameter defined as the droplet's kinetic versus surface tension; Capillary number, which is used to compare the viscose drag force and surface tension force; Bond number, which describes the gravity over surface tension. The solid surface's condition also needs to be examined to investigate the problem further, so the contact angle is critical.

There are multiple impact regimes, including deposition, splash, and rebound. For the deposition regime, the whole process can be divided into 4 phases: kinematic phase, spreading phase, oscillation/relaxation phase, and wetting phase.

The first kinematic phase is the initial contact between the moving droplet and the target substrate. During the initial contact, van de Waals force, interfacial tension, and

droplet inertia entangled each other, making this phase extremely complicated. Geometrically, the dynamic contact angle in this phase has a singularity at the beginning; Air bubbles may also be trapped beneath the drop, which randomly changes the oscillation and rebounding behaviors. Therefore, the research of this phase is mainly focused on the dynamic contact angle's variation and air bubble's trapping.

After that, the second phase, the spreading phase, is defined as the droplet's contact area on the solid continually spreading until reaching maximum. Depending on impact velocity and substrates, the spreading may evolve into different results. For industrial application concerns, the ultimate spreading factor is defined as the maximum spreading diameter versus the droplet's diameter. Previous studies have achieved modeling this phenomenon by different strategies.

The third phase, the oscillation/relaxation phase, is the regime in which the droplet starts to oscillate until damped off. During this phase, energy conservation between kinetic and surface tension continues, and the viscosity will finally absorb the kinetic energy within the drop. Satellite drop separation and body rebounding may occur at this phase if the substrate is hydrophobic or superhydrophobic. The droplet may also evolve into different splashes due to the asymmetric rim structure around the droplet. This phase provides an opportunity for analysis of the effect of each force in the dynamics by examining the oscillation frequencies and decay ratio of geometric properties such as flatness and dynamics contact angles.

The last phase, wetting, is the stage in which the oscillation has finally been dumped off, and the droplet's shape in the short term is considered stable. This phase is also

considered as directly related to industrial applications. Yet, the final statement is still affected by thermal transformation such as vaporizing and freezing or microfluidic phenomena like percolation. It is worth noting that the thermal or microfluid behavior at this phase will have an unpredictable influence on the substrate's wettability and change properties such as the contact angle randomly, increasing the complicities and uncertainty of analysis.

Our study is based on experimental observations. Phases 2 and 3 are mainly focused, yet the initial impact and pre-impact oscillating are also discussed in the post-processing phase. By assuming the viscosity as the damping effect of the system, we calculated the Reynolds numbers of each testing case. We created the model to represent the oscillation as a function of Re.

5.2 Experimental setting

5.2.1 Testing platform

We use shadowgraph imaging to observe the impact process. A high-speed camera with a frame per second (FPS) 2500 is mounted on the platform. A microscope lens is used to zoom the figures. The resolution of this imaging is 240 x 240 pixels. A led light with 1200 lumens brightness is used as the light source. A syringe pump drives the liquid into a syringe hanging above the testing surface; fluid accumulates around the needle's tip until it falls when gravity overcomes the capillary effect. Therefore, the impact velocity is controlled by setting the position of the syringe. The whole system is placed as the figure x1 shows

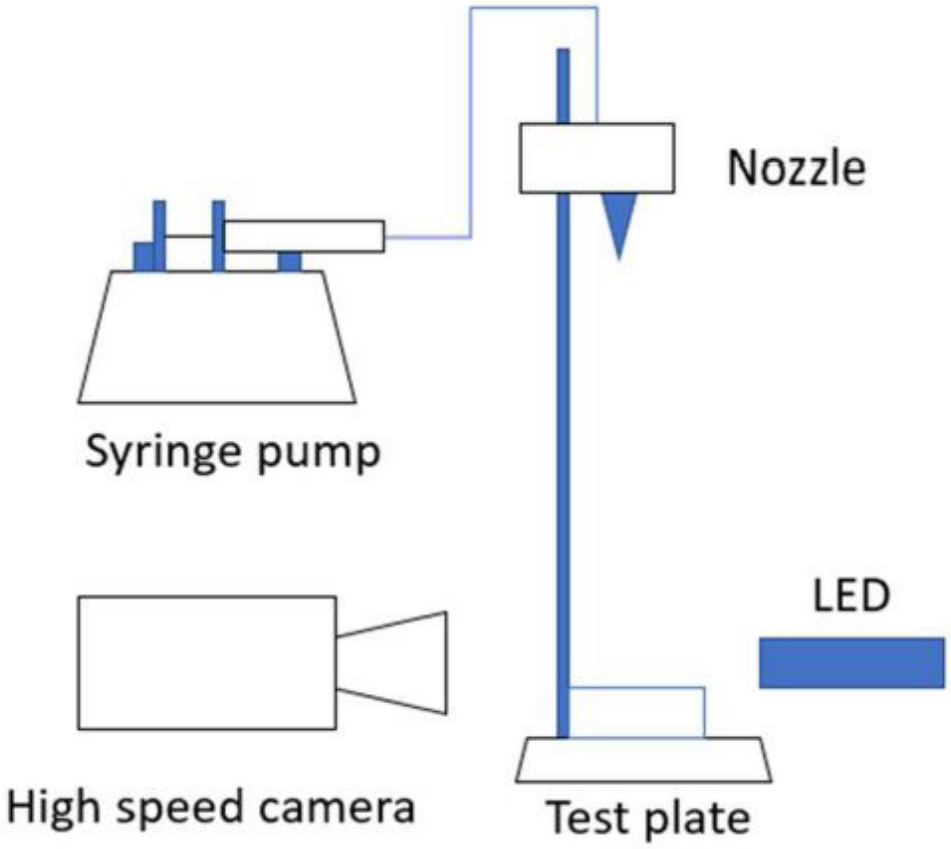

Figure 20. A testing platform for droplet impact studies

5.2.2 Material selection

To examine the influence of the Reynolds number on oscillation, we select liquids with different specific viscosity by using a mixture of deionized water and glycerol in the experiment setting. The viscosity changes for the binary mixture are not as sensitive as the surface tension. To filter the surface tension influence, we also select the water mixture of n-propane alcohol as the reference for the studies. The same kind of liquid under different impact velocities is also tested as the momentum is crucial for the Reynolds number.

Table 14. Test Matrix of selected solid material and liquids

Surface	ETFE	ETFE	ETFE	Glass	Glass	kapton	RainX	RainX
liquid	DI	p03	p05	DI	GD05	DI	DI	p03
SF	0.072	0.056	0.038	0.072	0.072	0.072	0.072	0.056
rho	0.998	0.994	0.99	0.998	1.0127	0.998	0.998	0.99
mu	1.002	1.009	1.014	1.002	1.235	1.002	1.002	1.009
D0	2.09	1.95	1.8	2.06	2.36	2.05	2.05	1.95
CA	97.3	80.04	57.84	45.3	93.8	74.07	96	77

We use multiple polymer solid materials as the testing substrates, including PTFE, ETFE, and ePTFE. Those materials are hydrophobic to water, making the testing results easier to observe, measure, and post-process.

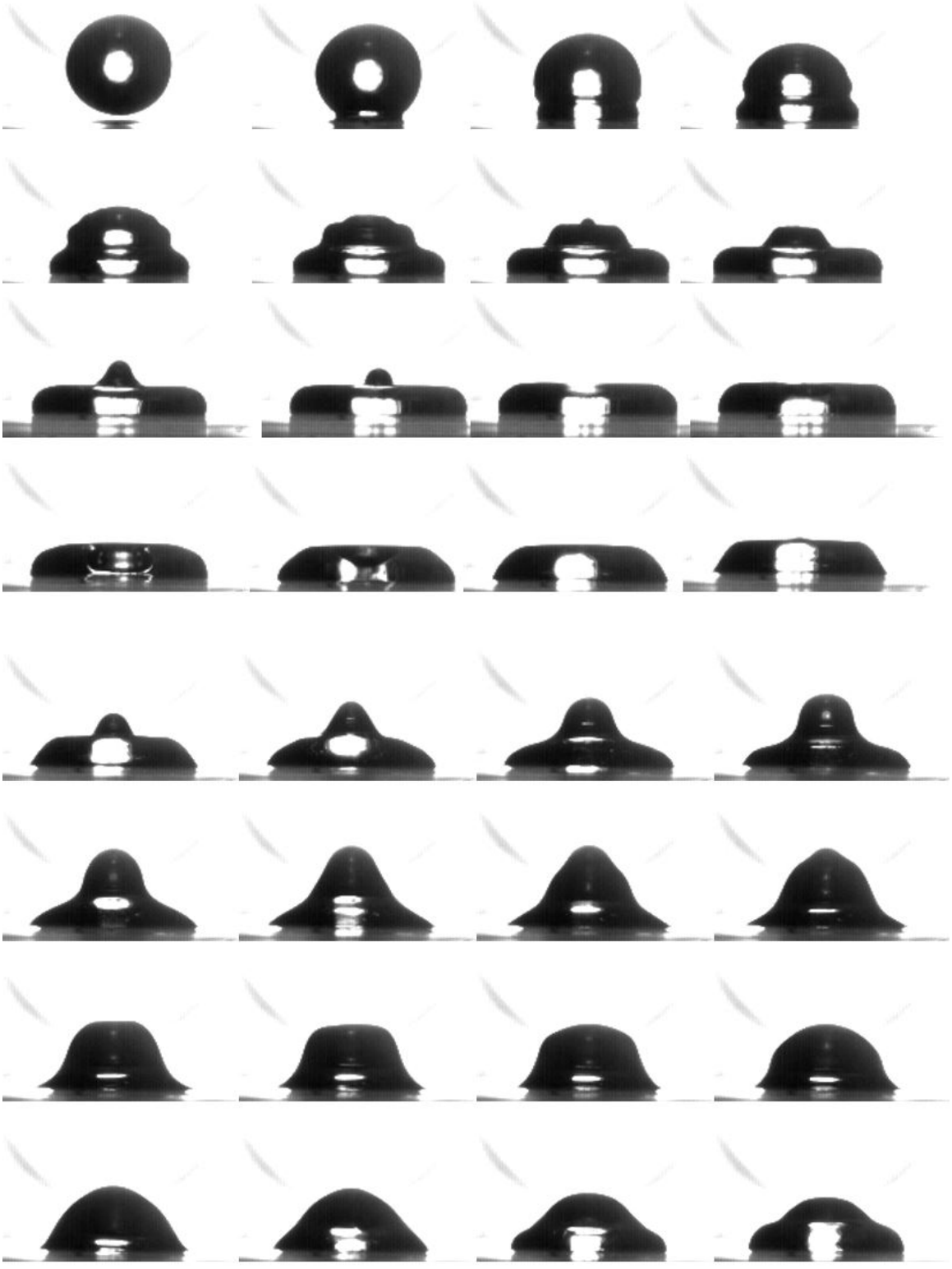

Figure 21. Deionized water impact on Kapton surface, with a velocity of 0.35m/s

5.3 Results

5.3.1 Oscillator model of a droplet impact system.

To study the impact dynamics, we apply the damped harmonic oscillator model (DHO) as the reference. In a typical DHO, the oscillation dynamics is the balancing between spring's stiffness, system's damping, and mass's inertia, as the following equations show:

$$m\frac{d^2x}{dt^2} + c\frac{dx}{dt} + kx = 0$$

Where the k is stiffness, c is the damping coefficient, and x is the location of the mass.

To specify the equation, we use decay rate λ, the most crucial factor. which is defined as $\lambda = \frac{c}{2m}$

Therefore, the oscillation frequencies can be calculated by solution:

$$\omega = \sqrt{\frac{k}{m} - \frac{c^2}{4m^2}}$$

Based on the damping ratio, we can formulate the damping conditions into 3 phases:

$\frac{k}{m} - \frac{c^2}{4m^2} < 0$ overdamped: parameter x continuously approaching the unreachable equilibrium state. Solution is

$$: x(t) = x_{amp}e^{-\lambda t}\left(c_1 e^{t\sqrt{\lambda^2-1}} + c_2 e^{-t\sqrt{\lambda^2-1}}\right)$$

$\frac{k}{m} - \frac{c^2}{4m^2} = 0$ critical damped: parameter x reaches the equilibrium state without across it. With such a solution:

$$x(t) = e^{-t}(c_1 + c_2 t)$$

$\frac{k}{m} - \frac{c^2}{4m^2} > 0$ underdamped: oscillation is significant, and the parameter has multiple chances to cross the equilibrium state. With a solution as follow:

$$x(t) = x_{eq} + A_x e^{-\lambda t}\cos(\omega t + \psi)$$

Here, x_{eq} is the equilibrium state of observed parameter x, A_x is the maximum amplitude of parameter x.

In the droplet problem, viscosity is the factor in absorbing the kinetic energy from oscillation, which is a stiffness-related parameter, specifically, decay rate and damped oscillation frequencies.

5.4 Testing results

5.4.1 Impact behaviors on high viscosity liquids

For binary mixtures of deionized water and glycerol, the surface tension of these mixtures has little change. The viscosities vary from 2.1 mNs/m^2 to 1.235 mNs/m^2. Such high viscosities provide a relatively low Reynolds number. Weber number, in these tests, has no significant difference from the DI water test under the same impact velocity.

From the prediction mentioned above, we notice that the oscillation decay rate of glycerol solution has a significant difference from the measurement. The higher the viscosity liquid mixture has, the more incompatible the model is for those cases.

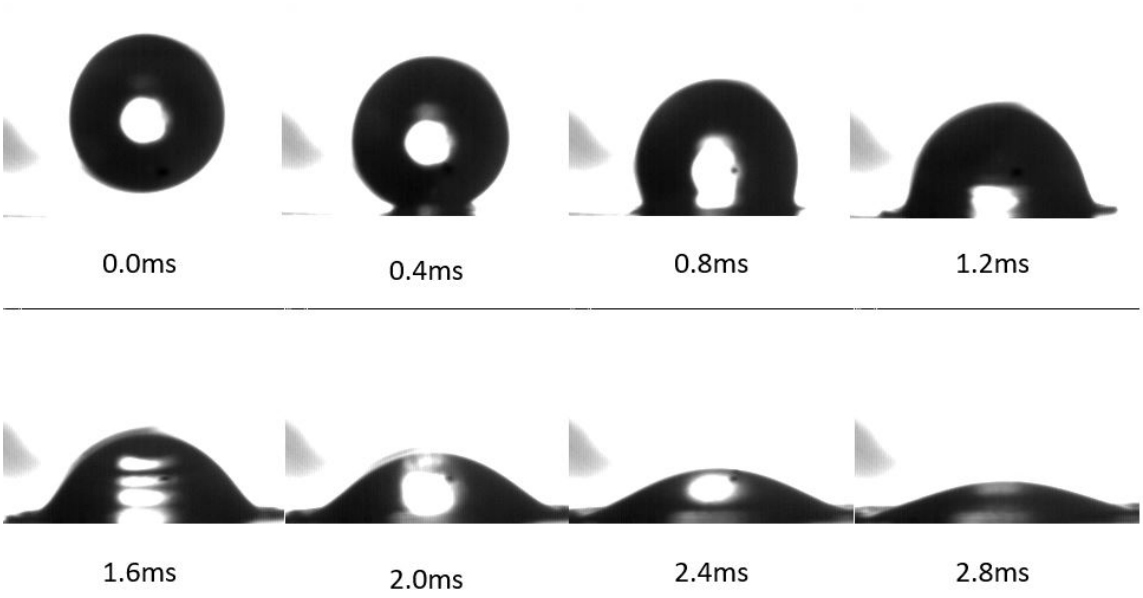

Figure 22.20% vol Glycerol mixture of water, deposited on the ePTFE surface, with a velocity of 1.05 m/s

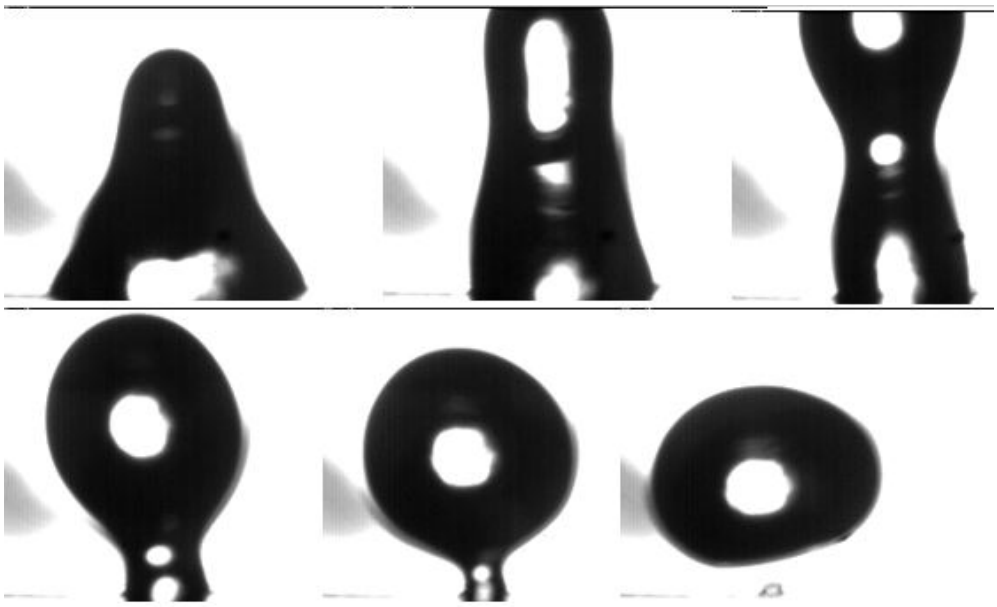

Figure 23. Rebounding Glycerol mixture on the ePTFE surface is a typical phenomenon that occurs on hydrophobic/ superhydrophobic surfaces.

One critical thing noteworthy is that the glycerol mixture of water shows hydrophobic on glass, which is different from pure deionized water conditions.

The glycerol-ePTFE testing results reveal the influence of viscosity on oscillations characteristics, especially the damping effect. Theoretically, as the viscosity increases, the damping coefficient of parameters such as flatness should be enhanced. However, the maximum damping coefficient occurs not at the highest viscosity regime but in the medium regime, around 1.459 Ns/m^2. The high viscosity condition (when viscosity is 2.15Ns/m^2) has an expected low damping coefficient. One potential explanation is the contact angle of glycerol mixture on ePTFE material has changed in the tests, and such wettability variation affects the droplet's oscillation range. The rebounding product

delays and elongates the oscillation period for high viscosity conditions, reducing the measurement's damping coefficient. Image resolution makes the damping effect easier to hide for a narrower range of oscillation.

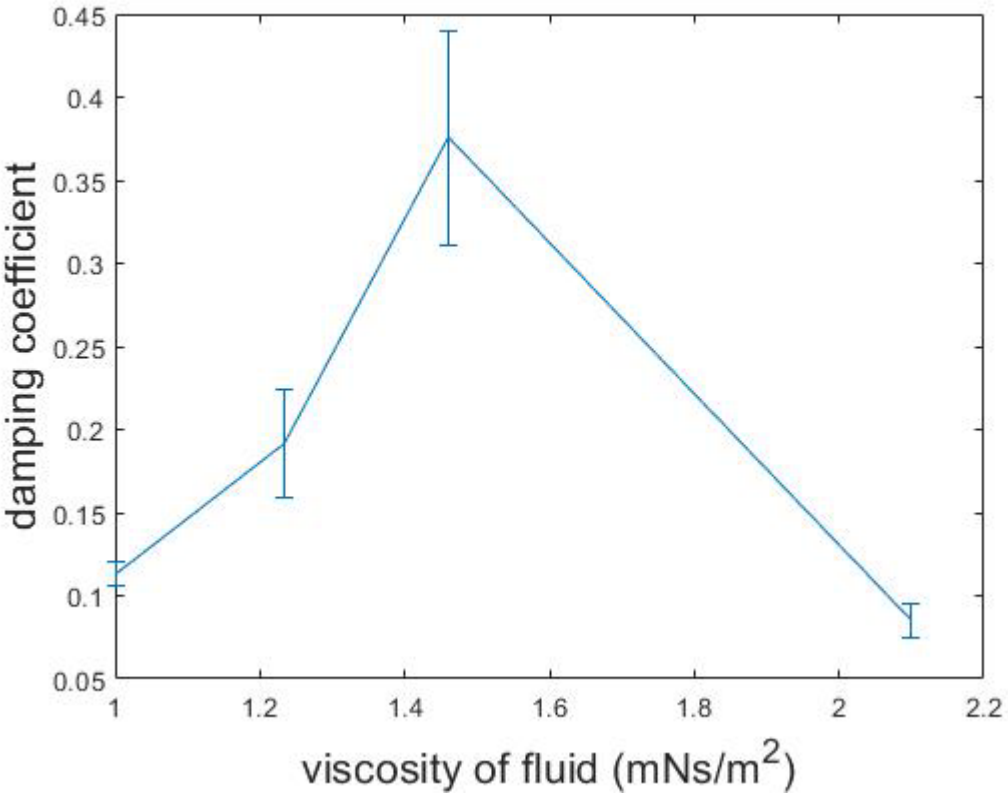

Figure 24. high viscosity fluid's damping coefficient of flatness.

5.4.2 Spreading velocity as a factor of oscillation

Young's equations reveal droplets' spreading and stabilizing dynamics as the balancing between interfacial tensions. However, in the impact process, the sudden added kinetic energy in this system will break the balancing and force the liquid's surface tension and

the solid's wettability to counter the impact of dynamic pressure. Such a re-balancing effect can be observed by analyzing the spreading velocity droplet.

The spreading contains two phases: the kinematic phase and the spreading phase. In the first phase, the spreading velocity of the contact line is hard to calculate due to the geometry of the droplet. Previous research has mentioned the initial spreading speed estimation, based on the geometry, the initial spreading speed of contact line is close to:$u_{init} = \frac{r_c}{t}$. As the impact process to the spreading phase, the velocity of the contact line is regulated by the minimum thickness of the liquid fil and the wettability.

According to the testing results, for most conditions, the average spreading velocity of droplets is lower than the initial impact velocity, except for some hydrophilic surface conditions. This is since surface tension of the liquid and solid wettability play as the counter force of spreading.

Table 15. Average spreading speed and impact velocity of testing results

Surface	liquid	velocity	spreading speed
ETFE	DI	0.99	0.70546875
ETFE	DI	1.1	0.7528125
ETFE	DI	1.16	0.890416667

ETFE	p03	0.99	0.47140625
ETFE	p05	0.52	0.688489583
ETFE	p05	0.99	0.783125
Glass	DI	0.52	0.470522727
Kapton	DI	0.35	0.4965
Kapton	DI	0.81	0.901794643
Kapton	DI	1.06	1.096892857
RainX	DI	0.52	1.39375
PTFE	DI	0.52	0.754892857
PTFE	DI	0.774	0.775321429
PTFE	DI	0.91	0.6159375
PTFE	DI	0.99	0.791607143
PTFE	DI	1.157	0.833392857
PTFE	DI	1.258	0.86
PTFE	p03	0.94	0.885

PTFE	p05	0.94	0.919875

5.4.3 Reynolds number's influence on oscillation.

From the model we introduce above, we can assume that the viscosity plays the kinetic energy consumer role, like the damper in the springe system. Thus, the decay rate of specific geometrical parameters (for example, flatness) should be a function of viscosity, as well as the impact velocity and mass. The following function can represent this:

$$\lambda = f(\rho, \mu, D, U)$$

Based on the dimension analysis, this equation become

$$\lambda_{dl} = f(Re)$$

Where the dimensionless decay rate $\lambda_{dl} = \frac{\lambda D}{U}$

Flatness is defined as the ratio of the droplet's height over the diameter. At the maximum spreading condition, due to the rim structuring, the measured size is most unlikely the size of the droplet's main body. Yet after that stage, the rim is absorbed back into the droplet's main body.

The most significant effects of viscosity on droplets' impact behavior reduced the oscillation frequencies and the damping enhancement. According to the experimental analysis, by increasing the Reynolds number of impact droplets, the decay rate of the drop's flatness continuously reduces, as the equations show:

$$f(Re) = 0.1783Exp(-0.0012Re) + (4.56e-6)Exp(0.0029Re)$$

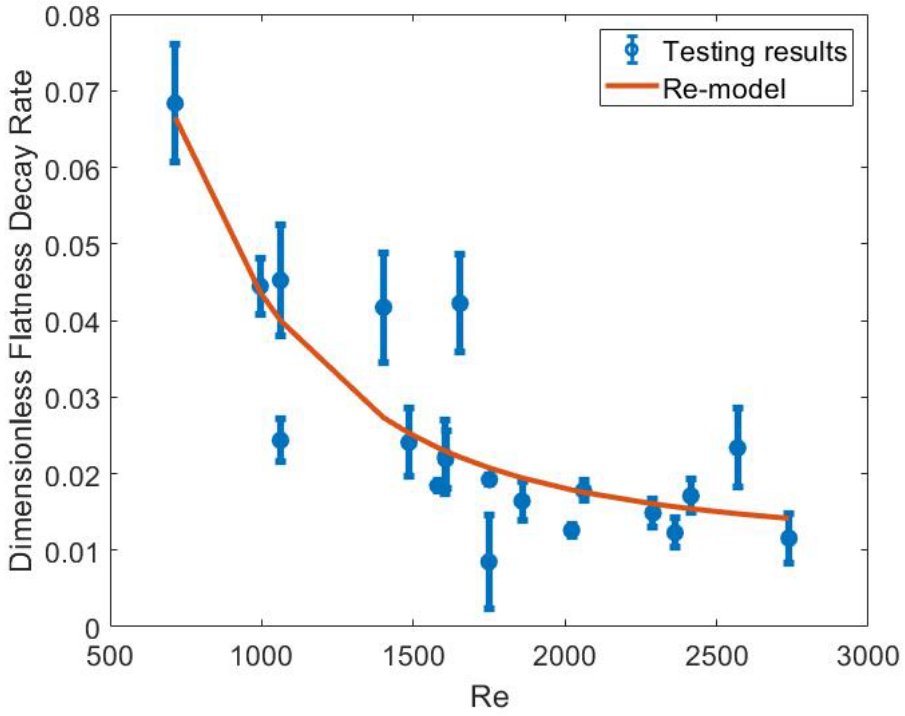

Figure 25. Droplet's flatness' decay rate (lambda) as a function of Reynolds number

The curve of this function shows that the viscosity significantly influences the damping when the Reynold number is relatively low. The decay rate continuously reduces until the Reynolds number is above 2000; then, it becomes stabilized. From the decay rate variation, we can estimate the damping coefficient as:

$$c = 2m\lambda = \frac{\pi}{6}\rho D_0^3 \lambda$$

We input the calculated decay rate into the test conditions to prove the estimation's accuracy, as the following figures show.

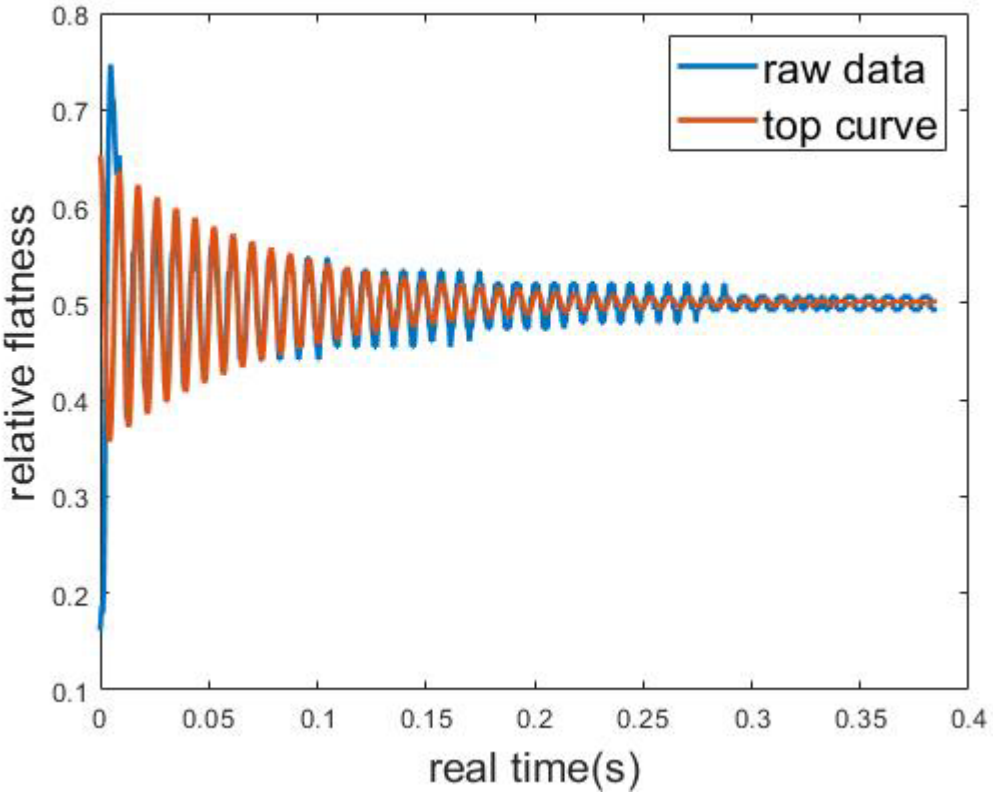

Figure 26. Deionized water deposited on the PTFE surface, with a velocity of 0.95 m/s

The damping coefficient of prediction has nicely matched the experimental results, especially at conditions of high surface tension liquid impact on hydrophobic surfaces, with mediate velocity. It is worth noting that this test curve's first "wave" has a much sharper shape and higher amplitude due to the complicated dynamics of the maximum

spreading stage. To examine the Reynolds number's impact on the oscillator model, separating the maximum spreading from the study is necessary.

5.5 Reynold and Weber number control the oscillation frequency.

From the DHO model, we can also assume that the oscillation frequency of droplets' parameters should be a function of both viscosity and surface tension. Based on the dimension analysis of oscillation frequency:

$$\omega = f_2(\rho, \mu, \sigma, U, D)$$

$$\omega = f_2\left(We, Re, \frac{U}{D}\right)$$

$$\omega_{dl} = \omega * \frac{D}{U} = f(We, Re)$$

Multiple potential fitting methods exist for oscillation frequencies. The following discussion is about the test of different strategies. Start with the Ohnesorge number:

$$Oh = \frac{\sqrt{We}}{Re}$$

After fitting the curve by the Gaussian function, the frequency function of the Ohnesorge number is as the flowing equation shows:

$$\omega_{dl} = 3.62 \times 10^{14} e^{-\left(\frac{Oh-2.31}{0.3982}\right)^2} + 2.0983 \times e^{-\left(\frac{Oh-0.0035}{8.8992\times10^{-4}}\right)^2}$$

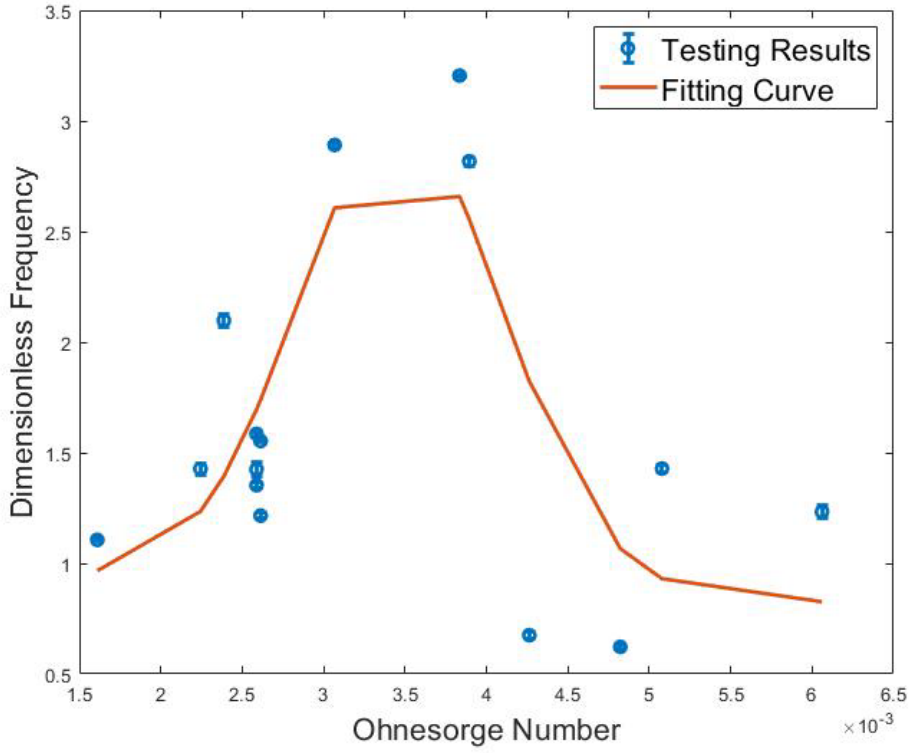

Figure 27. Oscillation frequency varies as Gaussian function of Ohnesorge number

This fitting strategy has been inaccurate in most conditions, especially at Ohnesorge number around 2.5.

Another fitting strategy is based on the variable as $We \times Re$, and for this type of curve, the frequency is as the following equations show:

$$\omega_{dl} = 3.7364 e^{-6.5877(We\times Re)\times10^{-5}} + 1.0481 e^{1.7189(We\times Re)\times10^{-6}}$$

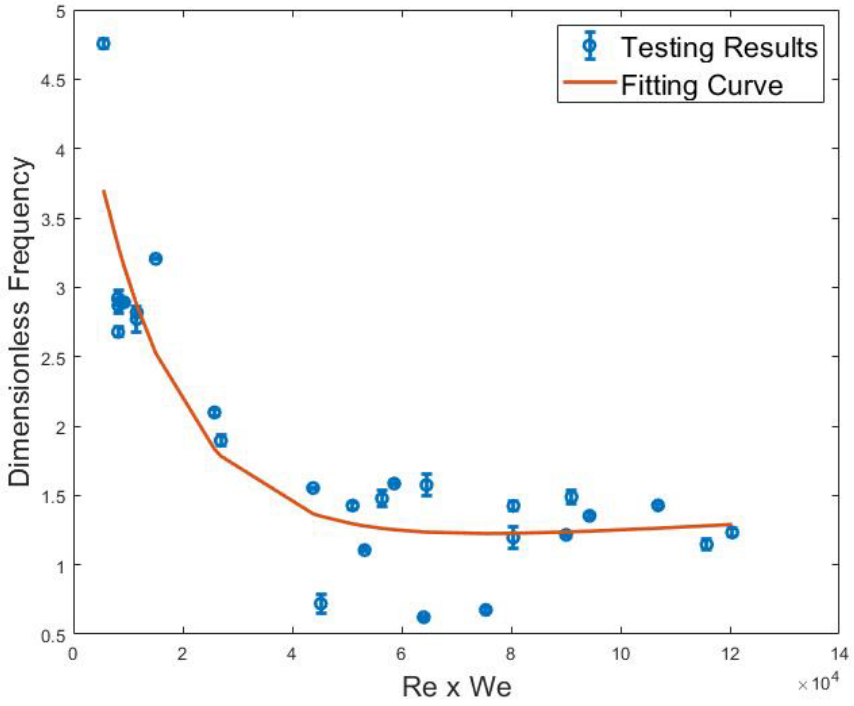

Figure 28. Oscillation frequency varies as a function of We x Re

The third fitting strategy is inspired by the expression of frequency in a DHO model. We assume a new factor K of We, Re

$$K = \sqrt{\frac{1}{Re} - \frac{1}{4We^2}}$$

Therefore, the third version of oscillation frequency expression is as the following equation:

$$\omega_{dl} = 10.2059\sqrt{\frac{1}{Re} - \frac{1}{4We^2}} - 0.3638$$

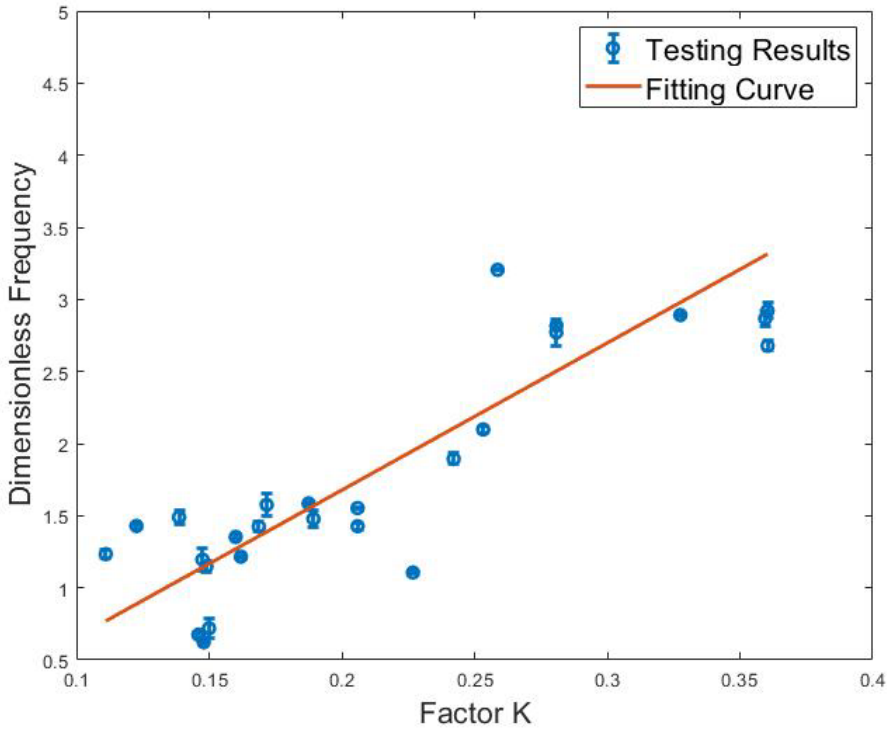

Figure 29. Oscillation frequency varies as a function of factor K

This linear function of factor K highly shows simplicity and similarity to the typical DHO model. Such expression can help us understand each variable's characters in this system.

To choose the appropriate model, we compare these expressions, examine the properties of those fitting, and select by fitting quality. According to the comparison,

the $We \times Re$ model with double term exponential functions expression has the highest quality, yet the linear approximation of factor K($\sqrt{\frac{1}{We} - \frac{1}{4Re^2}}$) is more straightforward to reveal the dynamics. Based on the study purpose, I would recommend linear fitting as the primary model for research.

Table 16. Fitting quality of different expression models

	SSE	R-square	adjusted R-square
$\sqrt{\frac{1}{We} - \frac{1}{4Re^2}}$	6.217	0.7387	0.7282
$We \times Re, exp2$	4.034	0.8304	0.8083
$We \times Re, exp1$	7.412	0.6884	0.676
Oh	13.84	0.4183	0.2798

With dimensionless parameter expressions of both oscillation frequency and damping completed, we can recreate the entire model to simulate the transient process of droplet's flatness oscillation, as the following expression shows:

$$x(\tau) = x_{eq} + A_x e^{\lambda(Re)\tau} \cos\left(\omega\left(\sqrt{\frac{1}{Re} - \frac{1}{4We^2}}\right)\tau + \psi\right)$$

$$\lambda(Re) = 0.1783e^{(-0.0012Re)} + (4.56e-6)e^{(0.0029Re)}$$

$$\omega\left(\sqrt{\frac{1}{Re}-\frac{1}{4We^2}}\right) = 10.2059\sqrt{\frac{1}{Re}-\frac{1}{4We^2}} - 0.3638$$

5.6 Unfitted and Special conditions

There are still some conditions where the damping coefficient prediction does not precisely match the results. When mixtures or temperature changes reduce the liquid's surface tension, the stiffness of the oscillator model will be diminished, too; as a result, the prediction based on the Reynold number has underestimated the potential influence of the Weber number. In such conditions, the model underestimated the decay rate of flatness. A noteworthy phenomenon is that in most unperfect matches, the average spreading velocity is higher than the droplet's impact velocity. Therefore, the kinematic phase of impact is also necessary to examine and discuss in future studies.

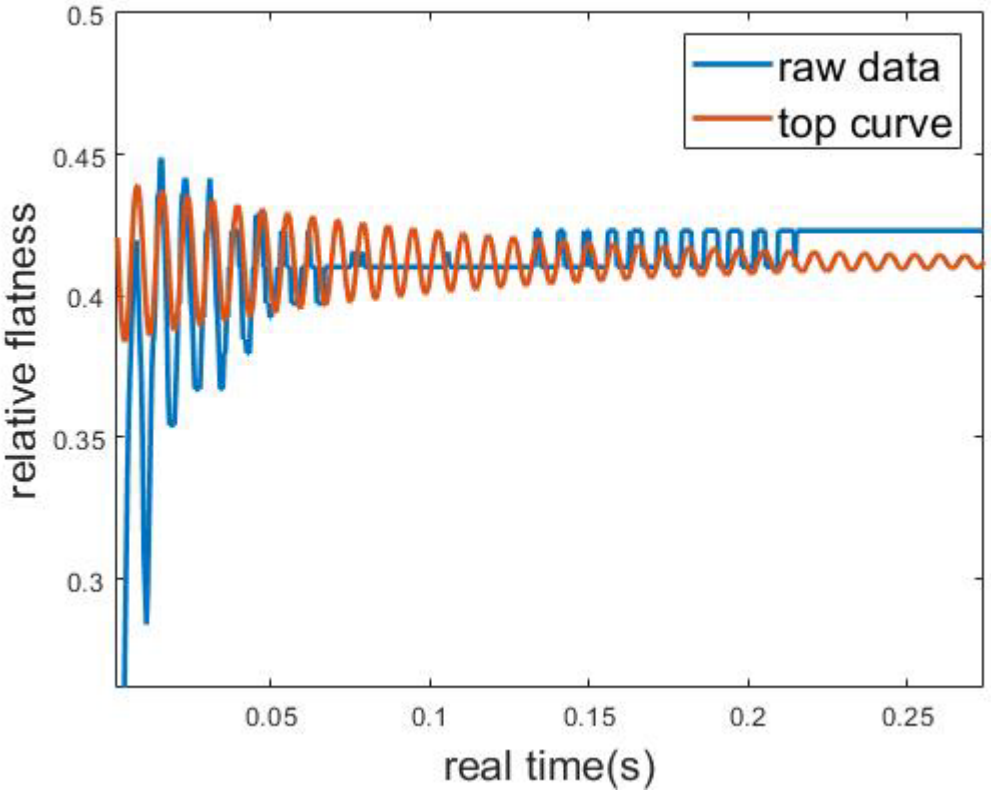

Figure 30. The flatness of water with a 3%vol mixture of alcohol on ETFE surface, at a velocity of 0.94m/s

Another unique condition is that the predicted decay rate still matches the results, but the testing shows overdamped characteristics. According to the oscillation dynamics, overdamped oscillation can be examined by the root of the frequency calculation.

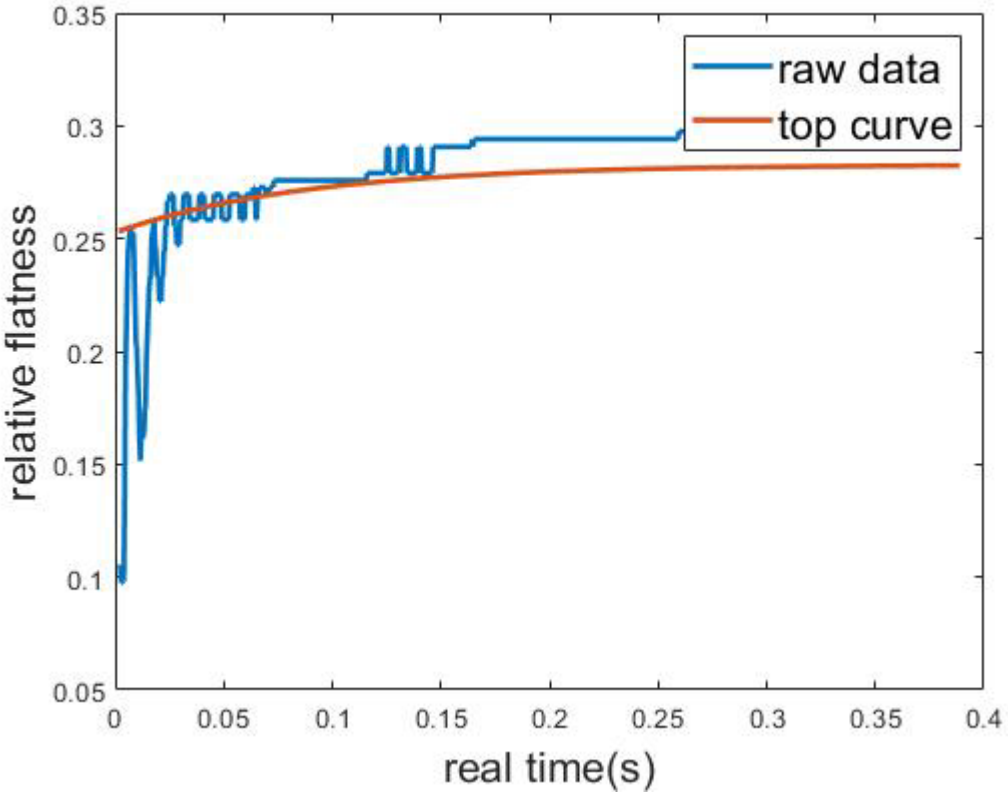

Figure 31. the flatness of water with 5% vol alcohol on ETFE surface, at a velocity of 0.91m/s

5.7 Conclusion of this section

In this article, we discussed how the Reynolds number influences the damping coefficient of droplet's geometric parameters, such as flatness. By creating the model of flatness as a binary exponential function of Re, we reveal how the decrement of Re enhances the damping effect. We also mention the averaging spreading of the droplet at kinematic and spreading phases and examine the influence of surface tension and wettability. Finally, we also said how fluid viscosity enhances the damping except for

the rebounding conditions. From the study, we can conclude that despite the crucial role of the Reynolds number, oscillation dynamics are not independent of surface conditions. Only focusing on viscosity change will not reveal the whole dynamics of such a phenomenon. Weber number must be included in the research, or the dynamics will not be applied for all many conditions. Future studies will examine the edge of the droplet's spreading and the potential vertex in the droplet's rim during the spreading phase.

6 Conclusion and recommendations for future planning

In my Ph.D. study program, I focused on the oscillation dynamics of droplet post-impact behaviors on the solid substrate. In chapter 3, I study the influence of Weber's number on the droplet's spreading and receding in the relaxation phase and create short-range models of both Weber's number and the equilibrium contact angle. In chapter 4, I reveal the dynamics of Weber number's effect on oscillation frequencies, as well as how the wettability of solid material limited the oscillation. I also briefly discuss the formation of hyperbolic crones at the axis of the droplet at the relaxation phase and the satellite droplet separation from the main body; such phenomena can be reviewed as the result of the droplet's internal vertex and the curvature changes. In chapter 5, my research includes the model of oscillations damping coefficient as an exponential function of Reynolds number, discusses how the wettability limited the spreading velocity, and how would viscosity enhance the damping effect on oscillation. For all these studies, I use a high-speed camera as the main tool and optical observation as the primary method.

However, this study still cannot observe and examine the internal structure of the droplet, especially the potential vertexes in the rim. I am also eager to monitor and measure the micrometer or nanometer-scale film around the droplet. So future studies may include the holography on droplet's plan view and the PIV method. I am also curious about the rebounding of the superhydrophobic substrate. Further investigation of this field shall include the model of rebounding as a function of Reynolds number or

otherwise. The droplet impact behavior is a vast and chaotic ocean of complicated phenomena, and my research is just a piece of the riffle.

7 Reference List

1. Chandra, S.; Fauchais, P., Formation of Solid Splats During Thermal Spray Deposition. *Journal of Thermal Spray Technology* **2009,** *18* (2), 148-180.
2. Pasandideh-Fard, M.; Pershin, V.; Chandra, S.; Mostaghimi, J., Splat Shapes in a Thermal Spray Coating Process: Simulations and Experiments. *Journal of Thermal Spray Technology* **2002,** *11* (2), 206-217.
3. Jadidi, M.; Moghtadernejad, S.; Dolatabadi, A., A Comprehensive Review on Fluid Dynamics and Transport of Suspension/Liquid Droplets and Particles in High-Velocity Oxygen-Fuel (HVOF) Thermal Spray. *Coatings* **2015,** *5* (4), 576-645.
4. Jabbari, F.; Jadidi, M.; Wuthrich, R.; Dolatabadi, A., A Numerical Study of Suspension Injection in Plasma-Spraying Process. *Journal of Thermal Spray Technology* **2014,** *23* (1-2), 3-13.
5. Mittal, G.; Paul, S., Suspension and Solution Precursor Plasma and HVOF Spray: A Review. *Journal of Thermal Spray Technology* **2022**.
6. Parizi, H. B.; Rosenzweig, L.; Mostaghimi, J.; Chandra, S.; Coyle, T.; Salimi, H.; Pershin, L.; McDonald, A.; Moreau, C., Numerical Simulation of Droplet Impact on Patterned Surfaces. *Journal of Thermal Spray Technology* **2007,** *16* (5-6), 713-721.
7. Yan, Z.; Zhao, R.; Duan, F.; Neng, T.; Chuan, K.; Fah, K.; Keong, P.; Sheng, Y., Spray Cooling. InTech: 2011.
8. Horacek, B.; Kiger, K. T.; Kim, J., Single nozzle spray cooling heat transfer mechanisms. *International Journal of Heat and Mass Transfer* **2005,** *48* (8), 1425-1438.
9. Jia, W.; Qiu, H.-H., Experimental investigation of droplet dynamics and heat transfer in spray cooling. *Experimental Thermal and Fluid Science* **2003,** *27* (7), 829-838.
10. Kim, J., Spray cooling heat transfer: The state of the art. *International Journal of Heat and Fluid Flow* **2007,** *28* (4), 753-767.
11. Gao, X.; Li, R., Spray impingement cooling: The state of the art. *Advanced Cooling Technologies and Applications* **2018**.
12. Sodtke, C.; Stephan, P., Spray cooling on micro structured surfaces. *International Journal of Heat and Mass Transfer* **2007,** *50* (19-20), 4089-4097.
13. Breitenbach, J.; Roisman, I. V.; Tropea, C., From drop impact physics to spray cooling models: a critical review. *Experiments in Fluids* **2018,** *59* (3).
14. Incropera, F. P.; DeWitt, D. P.; Bergman, T. L.; Lavine, A. S., *Fundamentals of heat and mass transfer*. Wiley New York: 1996; Vol. 6.
15. Liu, Y. C.; Farouk, T.; Savas, A. J.; Dryer, F. L.; Thomas Avedisian, C., On the spherically symmetrical combustion of methyl decanoate droplets and comparisons with detailed numerical modeling. *Combustion and Flame* **2013,** *160* (3), 641-655.
16. Cen, C.; Wu, H.; Lee, C.-F.; Liu, F.; Li, Y., Experimental investigation on the characteristic of jet break-up for butanol droplet impacting onto a heated surface in the film boiling regime. *International Journal of Heat and Mass Transfer* **2018,** *123*, 129-136.
17. Zama, Y.; Odawara, Y.; Furuhata, T., Experimental investigation on velocity inside a diesel spray after impingement on a wall. *Fuel* **2017,** *203*, 757-763.
18. Pei, Y.; Qin, J.; Li, X.; Zhang, D.; Wang, K.; Liu, Y., Experimental investigation on free and impingement spray fueled with methanol, ethanol, isooctane, TRF and gasoline. *Fuel* **2017,** *208*, 174-183.

19. Labergue, A.; Gradeck, M.; Lemoine, F., Experimental investigation of spray impingement hydrodynamic on a hot surface at high flow rates using phase Doppler analysis and infrared thermography. *International Journal of Heat and Mass Transfer* **2016,** *100*, 65-78.
20. Knausgård, K. Superhydrophobic anti-ice nanocoatings. Institutt for konstruksjonsteknikk, 2012.
21. Antonini, C.; Innocenti, M.; Horn, T.; Marengo, M.; Amirfazli, A., Understanding the effect of superhydrophobic coatings on energy reduction in anti-icing systems. *Cold regions science and technology* **2011,** *67* (1-2), 58-67.
22. Sarkar, D. K.; Farzaneh, M., Superhydrophobic coatings with reduced ice adhesion. *Journal of Adhesion Science and Technology* **2009,** *23* (9), 1215-1237.
23. Cao, L.; Jones, A. K.; Sikka, V. K.; Wu, J.; Gao, D., Anti-Icing Superhydrophobic Coatings. *Langmuir* **2009,** *25* (21), 12444-12448.
24. Moghtadernejad, S.; Jadidi, M.; Dolatabadi, A.; Esmail, N., SPH simulation of rivulet dynamics on surfaces with various wettabilities. *SAE International Journal of Aerospace* **2015,** *8* (1), 160.
25. Yi-Qiang, F.; Hong-Liang, W.; Ke-Xin, G.; Jing-Ji, L.; Dong-Ping, C.; ZHANG, Y.-J., Applications of modular microfluidics technology. *Chinese Journal of Analytical Chemistry* **2018,** *46* (12), 1863-1871.
26. Teh, S.-Y.; Lin, R.; Hung, L.-H.; Lee, A. P., Droplet microfluidics. *Lab on a Chip* **2008,** *8* (2), 198-220.
27. Lee, C.-Y.; Chang, C.-L.; Wang, Y.-N.; Fu, L.-M., Microfluidic mixing: a review. *International journal of molecular sciences* **2011,** *12* (5), 3263-3287.
28. Wijshoff, H., Drop dynamics in the inkjet printing process. *Current opinion in colloid & interface science* **2018,** *36*, 20-27.
29. Gan, H.; Shan, X.; Eriksson, T.; Lok, B.; Lam, Y., Reduction of droplet volume by controlling actuating waveforms in inkjet printing for micro-pattern formation. *Journal of micromechanics and microengineering* **2009,** *19* (5), 055010.
30. Castrejón-Pita, J.; Martin, G.; Hoath, S.; Hutchings, I., A simple large-scale droplet generator for studies of inkjet printing. *Review of Scientific Instruments* **2008,** *79* (7), 075108.
31. Yarin, A. L., DROP IMPACT DYNAMICS: Splashing, Spreading, Receding, Bouncing…. *Annual Review of Fluid Mechanics* **2006,** *38* (1), 159-192.
32. Josserand, C.; Thoroddsen, S. T., Drop Impact on a Solid Surface. *Annual Review of Fluid Mechanics* **2016,** *48* (1), 365-391.
33. Herbert, S.; Gambaryan-Roisman, T.; Stephan, P., Influence of the governing dimensionless parameters on heat transfer during single drop impingement onto a hot wall. *Colloids and Surfaces A: Physicochemical and Engineering Aspects* **2013,** *432*, 57-63.
34. Rein, M., Phenomena of liquid drop impact on solid and liquid surfaces. *Fluid Dynamics Research* **1993,** *12* (2), 61-93.
35. Marengo, M.; Antonini, C.; Roisman, I. V.; Tropea, C., Drop collisions with simple and complex surfaces. *Current Opinion in Colloid & Interface Science* **2011,** *16* (4), 292-302.
36. Ding, B.; Wang, H.; Zhu, X.; Chen, R.; Liao, Q., How supercooled superhydrophobic surfaces affect dynamic behaviors of impacting water droplets? *International Journal of Heat and Mass Transfer* **2018,** *124*, 1025-1032.
37. Bange, P. G.; Patil, N. D.; Bhardwaj, R. In *Impact Dynamics of a Droplet on a Heated Surface*, Proceedings of the 5th International Conference of Fluid Flow, Heat and Mass Transfer (FFHMT '18), Niagara Falls, ON, Canada, 2018; pp 7-9.
38. Liang, G.; Yang, Y.; Guo, Y.; Zhen, N.; Shen, S., Rebound and spreading during a drop impact on wetted cylinders. *Experimental thermal and fluid science* **2014,** *52*, 97-103.
39. Rioboo, R.; Tropea, C.; Marengo, M., Outcomes from a drop impact on solid surfaces. *Atomization Spray* **2001,** *11* (2), 155-165.

40. Rajesh, R. S.; Naveen, P.; Krishnakumar, K.; Ranjith, S. K., Dynamics of single droplet impact on cylindrically-curved superheated surfaces. *Experimental Thermal and Fluid Science* **2019,** *101*, 251-262.
41. Pan, Y.; Shi, K.; Duan, X.; Naterer, G. F., Experimental investigation of water droplet impact and freezing on micropatterned stainless steel surfaces with varying wettabilities. *International Journal of Heat and Mass Transfer* **2019,** *129*, 953-964.
42. Laan, N.; De Bruin, K. G.; Bartolo, D.; Josserand, C.; Bonn, D., Maximum Diameter of Impacting Liquid Droplets. *Physical Review Applied* **2014,** *2* (4).
43. Asai, A.; Shioya, M.; Hirasawa, S.; Okazaki, T., Impact of an Ink Drop on Paper. *J Imaging Sci Techn* **1993,** *37* (2), 205-207.
44. Chandra, S.; Avedisian, C. T., On the collision of a droplet with a solid surface. *Proceedings of the Royal Society of London. Series A: Mathematical and Physical Sciences* **1991,** *432* (1884), 13-41.
45. Jones, H., Cooling, Freezing and Substrate Impact of Droplets Formed by Rotary Atomization. *J Phys D Appl Phys* **1971,** *4* (11), 1657-+.
46. Mao, T.; Kuhn, D. C. S.; Tran, H., Spread and rebound of liquid droplets upon impact on flat surfaces. *Aiche J* **1997,** *43* (9), 2169-2179.
47. Pasandideh-Fard, M.; Qiao, Y. M.; Chandra, S.; Mostaghimi, J., Capillary effects during droplet impact on a solid surface. *Physics of Fluids* **1996,** *8* (3), 650-659.
48. Ukiwe, C.; Kwok, D. Y., On the Maximum Spreading Diameter of Impacting Droplets on Well-Prepared Solid Surfaces. *Langmuir* **2005,** *21* (2), 666-673.
49. Khojasteh, D.; Kazerooni, M.; Salarian, S.; Kamali, R., Droplet impact on superhydrophobic surfaces: A review of recent developments. *Journal of Industrial and Engineering Chemistry* **2016,** *42*, 1-14.
50. Gundersen, H.; Leinaas, H. P.; Thaulow, C., Surface Structure and Wetting Characteristics of Collembola Cuticles. *PLoS ONE* **2014,** *9* (2), e86783.
51. Tang, C.; Qin, M.; Weng, X.; Zhang, X.; Zhang, P.; Li, J.; Huang, Z., Dynamics of droplet impact on solid surface with different roughness. *International Journal of Multiphase Flow* **2017,** *96*, 56-69.
52. Phan, H. T.; Caney, N.; Marty, P.; Colasson, S.; Gavillet, J., Surface wettability control by nanocoating: the effects on pool boiling heat transfer and nucleation mechanism. *International Journal of Heat and Mass Transfer* **2009,** *52* (23-24), 5459-5471.
53. Kandlikar, S. G., A Theoretical Model to Predict Pool Boiling CHF Incorporating Effects of Contact Angle and Orientation. *Journal of Heat Transfer* **2001,** *123* (6), 1071-1079.
54. Kim, S. H.; Jiang, Y.; Kim, H., Droplet impact and LFP on wettability and nanostructured surface. *Experimental Thermal and Fluid Science* **2018,** *99*, 85-93.
55. Bobinski, T.; Sobieraj, G.; Gumowski, K.; Rokicki, J.; Psarski, M.; Marczak, J.; Celichowski, G., Droplet impact in icing conditions–the influence of ambient air humidity. *Archives of Mechanics* **2014,** *66* (2), 127-142.
56. Jadidi, M.; Farzad, M.; Trepanier, J.; Dolatabadi, A. In *Effects of ambient air relative humidity and surface temperature on water droplet spreading dynamics*, Fluids Engineering Division Summer Meeting, American Society of Mechanical Engineers: 2018; p V001T15A006.
57. Zhao, P.; Hargrave, G. K.; Versteeg, H. K.; Garner, C. P.; Reid, B. A.; Long, E.; Zhao, H., The dynamics of droplet impact on a heated porous surface. *Chemical Engineering Science* **2018,** *190*, 232-247.
58. Chen, H.; Cheng, W.-l.; Peng, Y.-h.; Jiang, L.-j., Dynamic Leidenfrost temperature increase of impacting droplets containing high-alcohol surfactant. *International Journal of Heat and Mass Transfer* **2018,** *118*, 1160-1168.

59. Hamdan, K. S.; Kim, D.-E.; Moon, S.-K., Droplets behavior impacting on a hot surface above the Leidenfrost temperature. *Annals of Nuclear Energy* **2015,** *80*, 338-347.
60. Yun, S.; Hong, J.; Kang, K. H., Suppressing drop rebound by electrically driven shape distortion. *Physical Review E* **2013,** *87* (3).
61. Yun, S.; Lim, G., Control of a bouncing magnitude on a heated substrate via ellipsoidal drop shape. *Applied Physics Letters* **2014,** *105* (24), 244108.
62. Yun, S.; Lim, G., Ellipsoidal drop impact on a solid surface for rebound suppression. *Journal of Fluid Mechanics* **2014,** *752*, 266-281.
63. Yun, S., Bouncing of an ellipsoidal drop on a superhydrophobic surface. *Scientific Reports* **2017,** *7* (1).
64. Yun, S., Impact dynamics of egg-shaped drops on a solid surface for suppression of the bounce magnitude. *International Journal of Heat and Mass Transfer* **2018,** *127*, 172-178.
65. Povarov, O.; Nazarov, O.; Ignat'evskaya, L.; Nikol'Skii, A., Interaction of drops with boundary layer on rotating surface. *Journal of engineering physics* **1976,** *31* (6), 1453-1456.
66. Mundo, C.; Sommerfeld, M.; Tropea, C., Droplet-wall collisions: experimental studies of the deformation and breakup process. *International journal of multiphase flow* **1995,** *21* (2), 151-173.
67. Zen, T.-S.; Chou, F.-C.; Ma, J.-L., Ethanol drop impact on an inclined moving surface. *International communications in heat and mass transfer* **2010,** *37* (8), 1025-1030.
68. Visser, C. W.; Pohl, R.; Sun, C.; Römer, G.-W.; Huis In 'T Veld, B.; Lohse, D., Toward 3D Printing of Pure Metals by Laser-Induced Forward Transfer. *Advanced Materials* **2015,** *27* (27), 4087-4092.
69. Demirci, U., Acoustic Picoliter Droplets for Emerging Applications in Semiconductor Industry and Biotechnology. *Journal of Microelectromechanical Systems* **2006,** *15* (4), 957-966.
70. Shojaeefard, M. H.; Khaneshan, V. M.; Ehteram, M. A.; Akbari, M.; Allymehr, E., Taguchi optimization of micron sized lubricant oil droplet deposition on a hot plate. *Journal of Mechanical Science and Technology* **2015,** *29* (8), 3277-3285.
71. Lee, S.; Mudawar, I., Enhanced model for annular flow in micro-channel heat sinks, including effects of droplet entrainment/deposition and core turbulence. *International Journal of Heat and Mass Transfer* **2019,** *133*, 510-530.
72. Feng, L.; Zhang, Z.; Mai, Z.; Ma, Y.; Liu, B.; Jiang, L.; Zhu, D., A Super-Hydrophobic and Super-Oleophilic Coating Mesh Film for the Separation of Oil and Water. *Angewandte Chemie* **2004,** *116* (15), 2046-2048.
73. Shum, H. C.; Abate, A. R.; Lee, D.; Studart, A. R.; Wang, B.; Chen, C.-H.; Thiele, J.; Shah, R. K.; Krummel, A.; Weitz, D. A., Droplet Microfluidics for Fabrication of Non-Spherical Particles. *Macromolecular Rapid Communications* **2010,** *31* (2), 108-118.
74. Wang, J.-T.; Wang, J.; Han, J.-J., Fabrication of Advanced Particles and Particle-Based Materials Assisted by Droplet-Based Microfluidics. *Small* **2011,** *7* (13), 1728-1754.
75. Šikalo, Š.; Marengo, M.; Tropea, C.; Ganić, E. N., Analysis of impact of droplets on horizontal surfaces. *Experimental Thermal and Fluid Science* **2002,** *25* (7), 503-510.
76. Rioboo, R.; Marengo, M.; Tropea, C., Time evolution of liquid drop impact onto solid, dry surfaces. *Experiments in Fluids* **2002,** *33* (1), 112-124.
77. Tarlet, D.; Allouis, C.; Bellettre, J., The balance between surface and kinetic energies within an optimal micro-explosion. *International Journal of Thermal Sciences* **2016,** *107*, 179-183.
78. Eggers, J.; Fontelos, M. A.; Josserand, C.; Zaleski, S., Drop dynamics after impact on a solid wall: Theory and simulations. *Physics of Fluids* **2010,** *22* (6), 062101.
79. Chubynsky, M. V.; Belousov, K. I.; Lockerby, D. A.; Sprittles, J. E., Bouncing off the Walls: The Influence of Gas-Kinetic and van der Waals Effects in Drop Impact. *Physical Review Letters* **2020,** *124* (8).

80. Thoroddsen, S. T.; Etoh, T. G.; Takehara, K.; Ootsuka, N.; Hatsuki, Y., The air bubble entrapped under a drop impacting on a solid surface. *Journal of Fluid Mechanics* **2005,** *545*, 203-212.
81. Bartolo, D.; Josserand, C.; Bonn, D., Retraction dynamics of aqueous drops upon impact on non-wetting surfaces. *Journal of Fluid Mechanics* **2005,** *545* (-1), 329.
82. Roisman, I. V., Inertia dominated drop collisions. II. An analytical solution of the Navier–Stokes equations for a spreading viscous film. *Physics of Fluids* **2009,** *21* (5), 052104.
83. Singh, M.; Haverinen, H. M.; Dhagat, P.; Jabbour, G. E., Inkjet Printing-Process and Its Applications. *Advanced Materials* **2010,** *22* (6), 673-685.
84. Patil, N. D.; Bhardwaj, R.; Sharma, A., Droplet impact dynamics on micropillared hydrophobic surfaces. *Experimental Thermal and Fluid Science* **2016,** *74*, 195-206.
85. Lin, S. J.; Zhao, B. Y.; Zou, S.; Guo, J. W.; Wei, Z.; Chen, L. Q., Impact of viscous droplets on different wettable surfaces: Impact phenomena, the maximum spreading factor, spreading time and post-impact oscillation. *J Colloid Interf Sci* **2018,** *516*, 86-97.
86. De Gennes, P. G., Wetting: statics and dynamics. *Reviews of Modern Physics* **1985,** *57* (3), 827-863.
87. Moghtadernejad, S.; Jadidi, M.; Tembely, M.; Esmail, N.; Dolatabadi, A., Concurrent Droplet Coalescence and Solidification on Surfaces With Various Wettabilities. *Journal of Fluids Engineering* **2015,** *137* (7), 071302.
88. Maretti; Rustichelli; Lassinantti, G.; Costantino; Siligardi; Miselli; Buttini; Montecchi; Leo; Truzzi; Iannuccelli, The Impact of Lipid Corona on Rifampicin Intramacrophagic Transport Using Inhaled Solid Lipid Nanoparticles Surface-Decorated with a Mannosylated Surfactant. *Pharmaceutics* **2019,** *11* (10), 508.
89. Clanet, C.; Béguin, C.; Richard, D.; Quéré, D., Maximal deformation of an impacting drop. *Journal of Fluid Mechanics* **2004,** *517*, 199-208.
90. Rotation of a rebounding-coalescing droplet on a superhydrophobic surface. *Physics of Fluids* **2019,** *31* (6), 062109.